Journal of Nuclear Materials 389 (2009) 1–22

Contents lists available at ScienceDirect

Journal of Nuclear Materials

journal homepage: www.elsevier.com/locate/jnucmat

Nuclear fuels – Present and future

D. Olander *

Department of Nuclear Engineering, University of California, Berkeley, California, United States

A B S T R A C T

The important developments in nuclear fuels and their problems are reviewed and compared with the status of present light-water reactor fuels. The limitations of LWR fuels are reviewed with respect to important recent concerns, namely provision of outlet coolant temperatures high enough for use in H_2 production, destruction of plutonium to eliminate proliferation concerns, and burning of the minor actinides to reduce the waste repository heat load and long-term radiation hazard. In addition to current oxide-based fuel rod designs, the hydride fuel with liquid–metal thermal bonding of the fuel-cladding gap is covered. Finally, two of the most promising Generation IV reactor concepts, the very high temperature reactor and the sodium fast reactor, and the accompanying reprocessing technologies, aqueous-based UREX+1a and pyrometallurgical, are summarized. In all of the topics covered, the thermodynamics involved in the fuel's behavior under irradiation and in the reprocessing schemes are emphasized.

1. Introduction

The history and future of the nuclear reactor designed for electricity production (and other uses) are shown in Table 1. In the US, the light-water reactors (LWRs) now in operation were designed and for the most part built in the decade of the seventies. This phase of nuclear reactor orders came to an abrupt halt with the advent of the Three Mile Island reactor accident. In the US there has been a 30-year lacuna in design and construction of any type of nuclear reactor.

The rapid rise in the cost of natural gas have made power plants using this fuel less desirable than it has been in the past. Coal-fired plants suffer from the carbon dioxide that they emit. Consequently, there has been a 'renaissance' of sorts of nuclear power, resulting in the US, of well over 20 applications for construction-and-operating licenses for Generation III reactors have been submitted to the Nuclear Regulatory Commission. However, no money has yet been invested for their construction.

The pressure of competing economically with electricity produced by burning coal and natural gas has driven current reactor operators to seek ever higher burnup of their fuel. The current fuel design has reached its limit at a burnup estimated to be ~80 MWd/kg U. In addition, light-water reactors produce outlet coolant water at a maximum temperature of ~320 °C, which limits the efficiency of converting heat to electricity to ~33% and precludes use as process heat for H_2 production.

Moreover, concerns that were not present when the current fleet of reactors was designed have arisen. The two most important are the need to burn the minor actinides (MA)[1] and the need to reprocess fuel in a manner that never exposes pure plutonium. The reason for the former is to reduce the radioactivity and heat generation rate of nuclear wastes at long storage times. Because of their long half-lives, the minor actinides remain after essentially all of the fission products have decayed. Containing plutonium in a mixture whose radioactivity is high enough to deter separation into weapons-purity material is referred to as proliferation resistance. These two needs are met by changing both the design of the reactor and its fuel and by the method of treating the spent fuel.

Several years ago, the US DOE and international collaborators selected for detailed study six advanced reactor systems and their accompanying reprocessing schemes. The reactor concepts are shown in Table 2. Three are fast-neutron reactors, in which moderating material is absent and three are thermal neutron reactors, which rely on moderators such as hydrogen or carbon to reduce the 1 MeV fission neutrons to ~0.03 eV thermal neutrons. Of the six, only the two that are most likely to be constructed are reviewed here. The first is the VHTR.

In this paper, the materials constraints of the current light-water reactors are described along with a new fuel that eases the burnup limitation. Finally, two of the so-called Generation IV reactor concepts and their associated reprocessing methods are reviewed.

* Fax: +1 510 526 0556.
E-mail address: fuelpr@nuc.berkeley.edu

[1] The minor actinides include Np, Am and Cm. If Pu is present with the MAs, the mixture is called transuranics (TRU).

0022-3115/$ - see front matter © 2009 Elsevier B.V. All rights reserved.
doi:10.1016/j.jnucmat.2009.01.297

Table 1
Genealogy of large nuclear reactors.

Generation I	First nuclear electricity: EBR-I, Shippingport (US), Magnox (UK),.....1950s–1960
Generation II	Current fleet of LWRs – pressurized water (PWR) or boiling-water (BWR) (US); VVER (Russia); CANDU (a heavy-water cooled reactor) (Canada).....1970–1980
Generation II+	Current LWRs with new fuel; MOX, hydride fuel; liquid–metal bond
Generation III	LWRs of completely new design – passive safety, fewer valves, shorter piping: ABWR (GE-Toshiba), AP1000 (Westinghouse-AREVA); EPR (Europe) 1990 – present
Generation IV	Completely new designs or resuscitation of old reactor types – sodium fast reactor; (SFR); very-high-temperature reactor (VHTR)...2025 – ??

Table 2
Generation IV reactors.

Reactor Coolant	Neutron energy	Purpose: electricity +:
Helium	Fast	H_2 production
Lead-bismuth	Fast	Encapsulated, 30-year life, small reactor; BREST
Molten fluoride Salt	Thermal	Safety; H_2 production
→ Sodium	Fast#	Burner of minor actinides from light-water reactors
Supercritical Water	Thermal	higher electrical efficiency than current LWRs (H_2)
→ Helium	Thermal&	Very-high temp. process heat (e.g. for H_2 production)

E_n ~ 1 MeV & E_n ~ 0.025 eV

2. Generation II fuel assemblies and fuel elements for light-water reactors

A LWR reactor core is comprised of *fuel assemblies* in an arrangement that satisfies the following requirements:

(i) to provide a rigid structure for holding the *fuel elements*,
(ii) to deliver the desired thermal power to the coolant,
(iii) to provide a critical assembly with a minimum of neutron leakage,
(iv) to provide adequate coolant flow to remove fission heat and sufficient coolant volume for thermalization of fission neutrons by hydrogen.
(v) to accommodate control rods that maintain criticality as the fuel is consumed.

Fig. 1 shows a generic LWR fuel element. It consists of a ~4 m length of a zirconium–tin alloy tube with an OD of ~1.2 cm for boiling-water reactor (BWR) fuel rods and 0.8 cm OD for PWR rods. This cladding tube is filled with a ~3 m stack of fuel pellets, either UO_2 with uranium enrichments up to 5% or a mixture of UO_2 and PuO_2 (MOX). The remaining space above the fuel stack is an open volume called a *plenum*, which is designed to accommodate fission gas released from the fuel without overpressurizing the cladding.

2.1. Fretting failure of the cladding

Fig. 2 shows a cutaway drawing of the fuel assembly of a pressurized water reactor (PWR) and a very important component, the *grid spacer* through which the fuel rods pass. The cladding tubes are fixed in the grid spacer by *rod holders*, of which three types are shown. The design of rod holders is a true engineering compromise. If held too tightly, vertical thermal expansion of the rods due to temperature changes is impeded; if the rods are not firmly gripped, flow-induced vibration of the rods within the grid occurs. In either case, a fretting breach of the cladding as shown in the figure can result. This is the principal cause of cladding failure of LWR fuel rods.

2.2. Coolant chemistry

PWR coolant contains:

- *boric acid* enriched in B^{10} for nuclear reactivity control,
- *lithium hydroxide* to minimize corrosion by adjusting the pH,
- *zinc* (added as an organometallic compound) to reduce the transfer of radioactivity from the fuel rods to walls of the coolant circuit,
- *hydrogen* to remove highly-oxidizing species created by radiolysis of water.

Solid solutes cannot be added to BWR coolant water because vaporization at the upper portion of the fuel assembly would result in accumulation of the solutes in the liquid. However, hydrogen treatment is standard practice.

2.3. Cladding corrosion

Despite the above adjustment of the water chemistry, severe corrosion occasionally occurs, as shown in Fig. 3. The left hand photograph shows the type of corrosion observed on BWR cladding. The white spots are ZrO_2 which was formed by ingress of water through cracks in the otherwise intact oxide film. This phenomenon is termed *nodular corrosion*.

Because the cladding OD temperatures are higher in a PWR (by about 20 °C), *uniform corrosion* is more extensive than on BWR cladding. In addition, a mixture of iron and chromium spinel called CRUD collects on the cladding from deposition of Fe, Ni and Cr ions that have entered the coolant by corrosion of stainless steel piping in the primary coolant loop. This layer, which is not a corrosion layer, is harmful for two reasons. First, it can occlude boron from solution and alter the axial neutron-flux distribution. Second, it can release radioactive transition-metal nuclides that plate out at downstream locations in the primary circuit. The uniform corrosion layer beneath the CRUD is limited to a thickness of 100 μm. More extensive corrosion reduces the tube cross-section sufficiently to increase the stresses in this component.

2.4. Hydrogen embrittlement

The second consequence of corrosion, particularly in PWRs, is absorption of ~15% of the corrosion-product hydrogen in the substrate metal, as shown in the lower photograph of Fig. 3. The terminal solubility of hydrogen in zirconium is sufficiently low that platelets of zirconium hydride precipitate out, resulting in a significant loss of ductility.

2.5. Pellet-cladding interaction

As a result of fission of an atom of uranium into two fission product atoms, the fuel swells during irradiation. In addition, the steep temperature gradient in the fuel pellet generates thermal

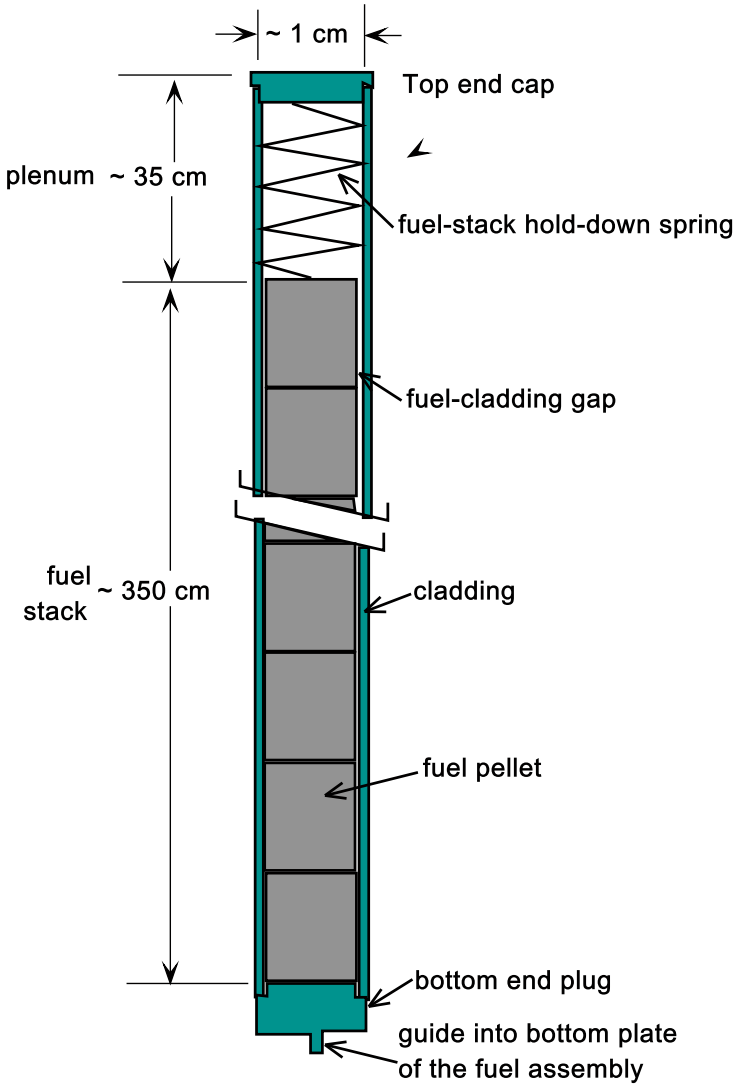

Fig. 1. A generic LWR fuel element.

stresses that exceed the fracture stress of UO_2. The result is pellet cracking shown schematically in Fig. 4. The 'hourglass' shape of the pellet is due to the switch from plane-strain conditions near the pellet midplane to plane-stress at the upper and lower faces. When fission-product swelling closes the fuel-cladding gap, the cladding pellet deforms into a shape reflecting that of the pellet. In addition to resembling a bamboo stalk, the cladding is stressed in tension both azimuthally and axially. The stressed cladding can fail in two ways. First, embrittlement due to hydrogen precipitates permits the stress to initiate cracking on the cladding OD. Second, the chemical effect of fission products such as iodine and cadmium on incipient cracks in the cladding ID can result in stress-corrosion cracking. This phenomena is termed *pellet-cladding interaction* (PCI), and remains a non-negligible source of cladding failures during operation.

Fig. 5 shows a typical stress-corrosion crack in the cladding. In addition to the uniform stresses engendered by pellet expansion, localized stresses are built up in regions where a piece of the pellet is missing, usually due to chipping during fabrication. This missing pellet fragment, if next to a crack in the fuel, is an especially potent source of PCI. The crack in the fuel facilitates movement of the dangerous fission products from the hot center of the pellet where release occurs to the fuel-cladding interface and from there to the tip of the crack in the cladding. Here the ductile metal is converted to the metal iodide ZrI_4, which is brittle and by rupturing easily, facilitates progression of the crack.

2.6. Fission gas release

Two deleterious phenomena result from release of the fission gases Kr and Xe from the fuel. The first concerns the portion that accumulates in the fuel-cladding gap, where the heavier rare gases replace some of the original helium. The consequence is a greatly reduced thermal conductivity of the gas. If the gap has not been closed by fuel swelling, this admixing causes the fuel temperature to rise, which in turn results in increased release of fission gas. This 'bootstrapping' effect can result in excessively high fuel temperatures and larger-than-usual fission-gas release fractions.

The second life-limiting feature arises from the fission gases that accumulate in the plenum (Fig. 1). If the added gas causes the pressure here to exceed the coolant pressure, the cladding 'lifts off' the fuel, thereby increasing the gap size and its thermal resistance.

2.7. Life-limiting phenomena

Any one these phenomena, namely fretting wear, cladding corrosion, hydrogen embrittlement, pellet-cladding interaction or

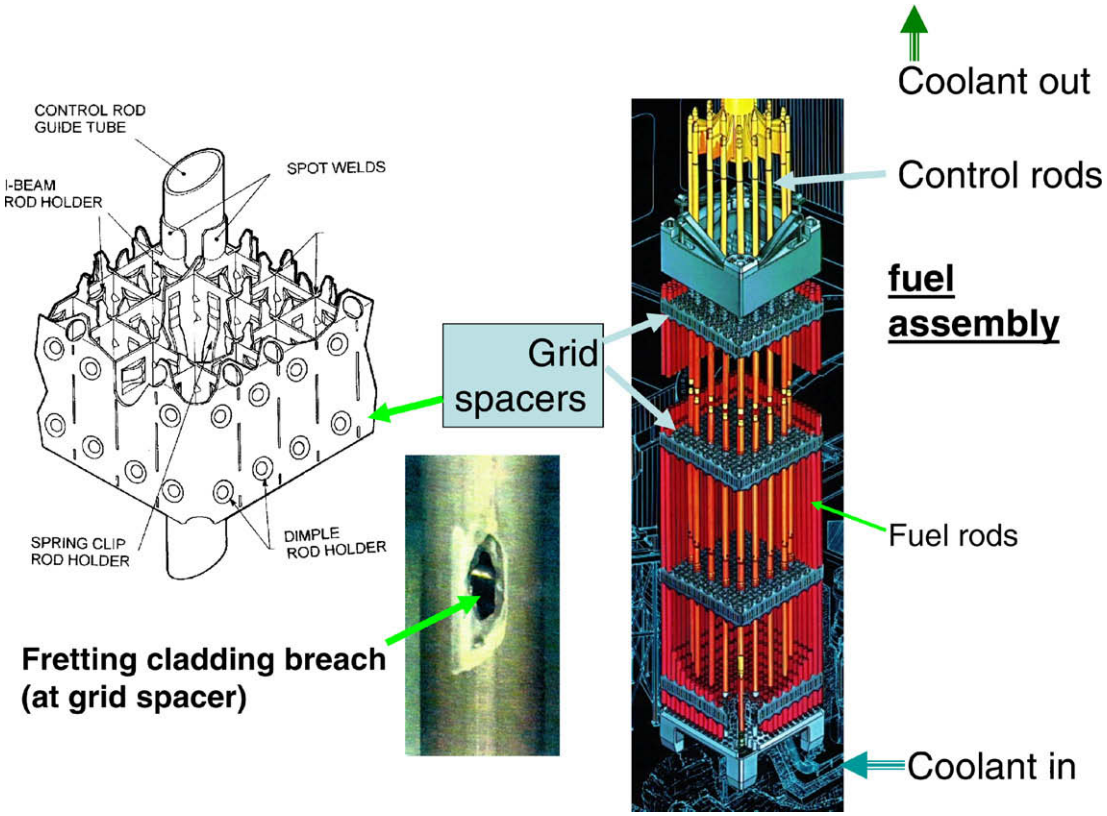

Fig. 2. Fuel assembly and grid spacer of a PWR.

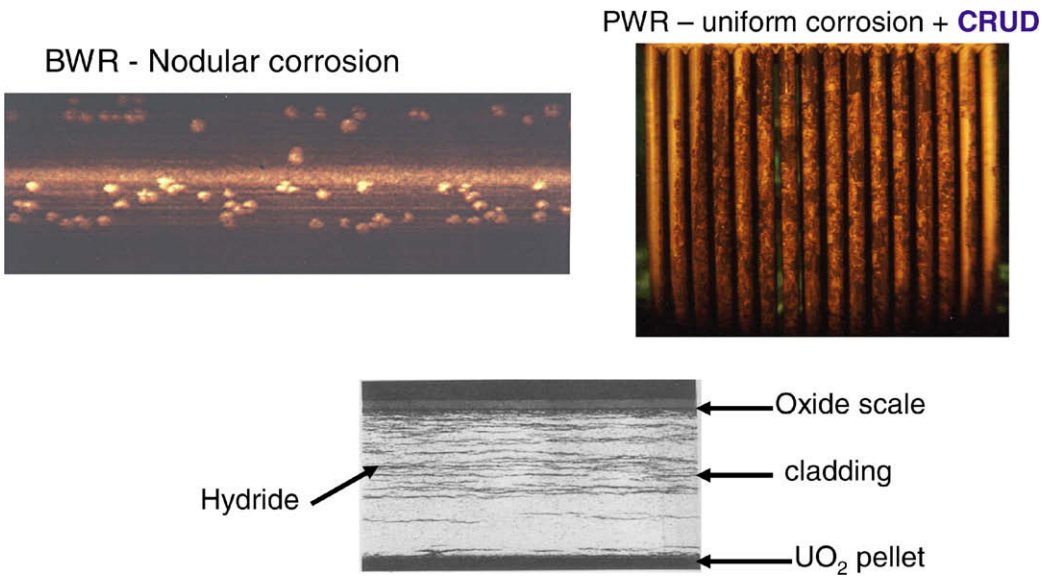

Fig. 3. Corrosion of zirconium-alloy LWR cladding.

excessive internal pressure due to fission-gas release, can be life-limiting for LWR fuel elements. The maximum burnup of current fuel designs is ~60 MWd/kg U. At greater burnups, the probability of a cladding failure becomes significantly larger than the current value of $\sim 10^{-5}$. Rupture of the cladding of a single fuel element in the core is more of an economic concern than a safety issue. Release of fission products and fuel through the breach in the cladding spreads radioactivity throughout the primary coolant circuit, necessitating reactor shutdown, replacement of the fuel assembly containing the defective fuel rod and extensive decontamination of exposed components.

3. Generation II+ advanced fuels for LWRs

3.1. Mixed U–Pu oxide (MOX)

Until now, the only fuel other than UO_2 that has been burned in LWRs is the mixed oxide $(U,Pu)O_2$. This fuel does not require iso-

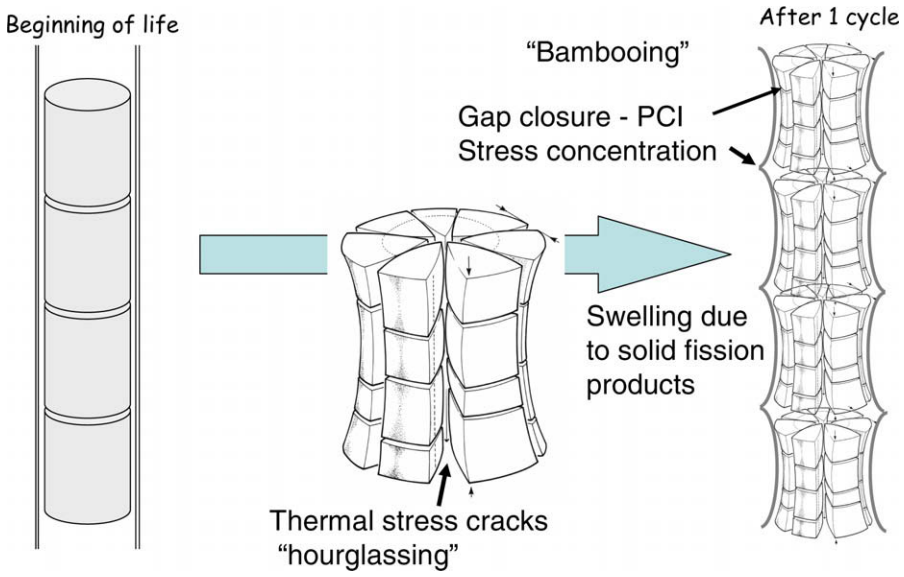

Fig. 4. Effects of fuel swelling and thermal stresses.

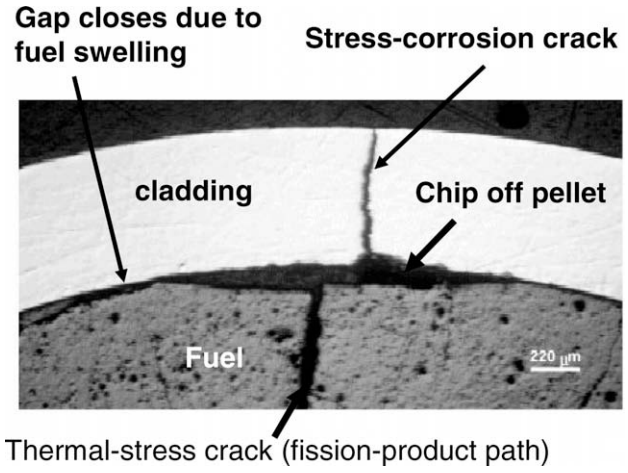

Fig. 5. Consequences of pellet-cladding interaction (PCI).

tope enrichment and serves as a means of disposing of plutonium from weapons programs and recycled Pu from reprocessing of spent LWR fuel. Its irradiation performance is no better than that of UO_2, and may even be less desirable. Depending on the method of fabricating MOX fuel, the microstructure may a three-phase system with dispersed PuO_2 and UO_2 particles embedded in a mixed oxide matrix [1] or a two-phase material with $(U,Pu)O_2$ particles in a continuous UO_2 phase [2]. Fig. 6 shows electron microprobe pictures of the MOX microstructures of the two types. The large white spots are the Pu-rich particles where the bulk of the fissions occur.

In some but not all reports, fission gas release from MOX is higher than that from UO_2, mainly because its thermal conductivity is ~10% lower, thereby increasing fuel temperature. Fig. 7 shows the scanning-electron microscope and optical microscope images of high-burnup regions of the two-phase type of MOX described above. The SEM image reveals large bubbles of fission gas in a plutonium-rich agglomerate close to the cladding inner surface. Optical image (b) shows precipitates of noble-metal fission products in the same region. Fuel-cladding contact is so intimate that a mixed $(U,Zr)O_2$ layer has developed on the inner Zircaloy surface.

In addition, the ratio of the fissile isotopes $^{239}Pu + {}^{241}Pu$ to the non-fissile isotopes $^{240}Pu + {}^{242}Pu$ decreases with each plutonium recycle. This requires increasing total Pu loadings to maintain criticality [3]. A maximum Pu/U + Pu ratio of 0.1 is permitted in order to avoid a positive void coefficient. On the favorable side, the creep rate of MOX is greater than that of UO_2, which results in reduction of the bambooing effect shown in Fig. 4 and the consequent risk of cladding failure by excessive hoop stress on the cladding.

3.2. Hydride fuel with a liquid–metal bond

This fuel combines features from two very different reactors into a promising new fuel for LWRs. Instead of UO_2 or MOX, the fuel is the hydride of uranium and zirconium, $(U_{0.31}Zr)H_{1.6}$ [4]. This fuel consists of particles of metallic uranium dispersed in a matrix of $ZrH_{1.6}$ (Fig. 8). It powers the well-known TRIGA research reactors [5].

Advantages of the hydride over the oxide fuel include:

- a part of the moderator (H) is in the fuel; not all moderation need be provided by the hydrogen in the coolant. This is especially important in BWRs, where the upper reaches of the core are filled with steam, which has very little capacity for moderating neutrons. Even in a PWR, the coolant channel cross-section can be reduced because the water is needed more for cooling than for moderation of neutrons. In both cases, the fuel rods can be more closely packed, which reduces the volume of both the core and the pressure vessel.
- Higher burnup can be attained in a hydride-fueled LWR than in one with oxide fuel [6].
- The negative reactivity feedback in a transient is faster with hydride fuel than with oxide fuel (TRIGA reactors are routinely pulsed by rapid control rod withdrawal).
- The thermal conductivity of the hydride is ~6 times greater than that of UO_2, and is much less temperature-dependent [5]. Consequently, for a linear power of 375 W/cm, for example, the maximum fuel temperature is <700 °C. For an oxide fueled rod operating at the same linear power, the maximum temperature would be close to 2100 °C. The low fuel temperature of hydride fuel significantly reduces stored energy and fission product release.

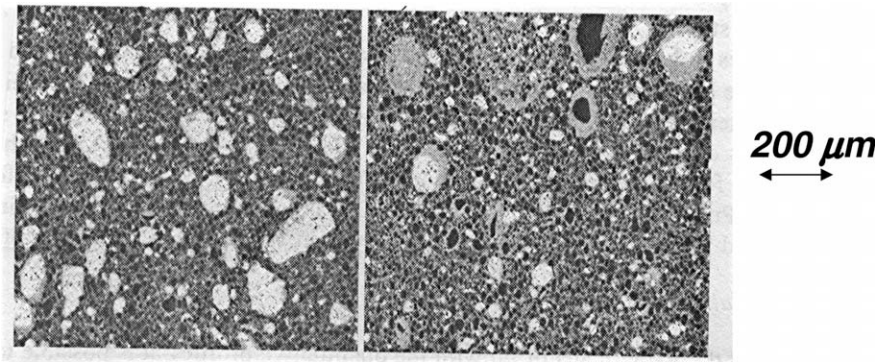

Fig. 6. Electron microprobe images MOX fabricated by two methods [1].

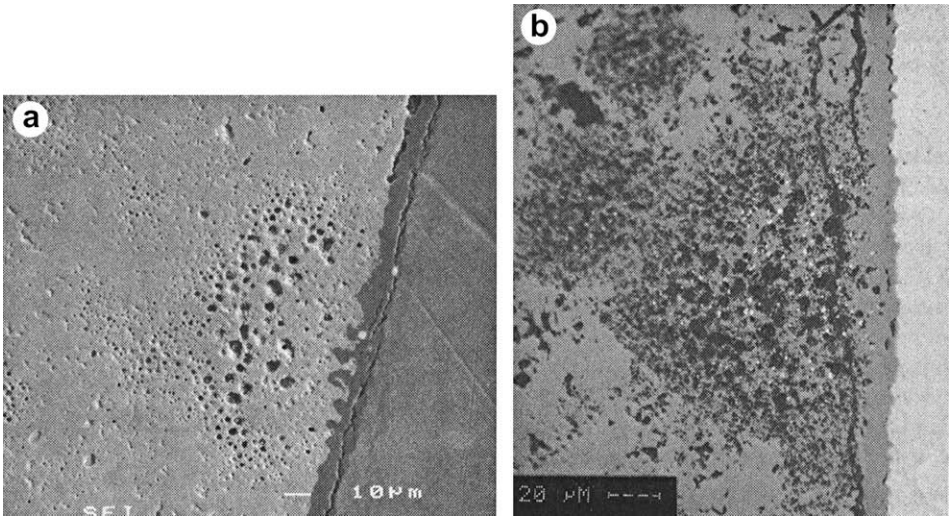

Fig. 7. SEM (a) and optical microscope (b) images of a former Pu-rich agglomerate in high-burnup MOX [2].

Selection of the initial gap thickness has always been a concern with helium-filled oxide fuels. The gap must be wide enough to accommodate fuel swelling without cladding strain in excess 1% after the gap closes. Yet it must by sufficiently narrow to avoid an excessively-large temperature drop across the gap. The compromise is an initial gap thickness of ~80 μm. With this size, the gap closes after about 1 year of irradiation, and thereafter fission-product swelling continues to strain the cladding.

A second problem with helium bonding of the fuel-cladding gap is that prepressurization of the rod during fabrication of ~20 atm is required. The reason is that with a lower He concentration, mixing with released fission gas (mainly Xe) would degrade the thermal conductivity of the gas to an unacceptable level.

In order to maintain a sufficiently low fuel temperature in a hydride-fueled rod, helium cannot be used as a thermal bond in the fuel-cladding gap. Instead, a low-melting (~120 °C) metal alloy consisting of equal parts by weight of lead, tin and bismuth is the gap filler. As a liquid, this material has a thermal conductivity that is 100 times greater than that of helium, which essentially eliminates the gap thermal resistance. The alloy does not react with water and has a very low neutron cross-section. Several important advantages result from the use of a liquid metal (LM) in the gap.

- At a linear heat rate of 375 W/cm, the maximum fuel temperature is reduced to ~550 °C from ~700 °C with a helium bond [4], resulting in practically no thermal release of fission gases.
- The liquid metal protects the cladding ID from noxious fission products, which, as shown in Fig. 5, is not possible with helium.
- With liquid–metal bonding, the initial gap thickness can be made wide enough to prevent contact of fuel and cladding for the entire lifetime of the fuel element [7]. This means that the cladding is never stressed in tension, so cracking of the type shown in Fig. 5 is avoided.
- In the event of a cladding breach, such as the fretting hole shown in Fig. 1, the LM in the gap is blown into the plenum by the inrush of coolant, which flashes to steam. However, the LM beneath the breach is unaffected, and prevents ingress of steam to the bottom of the rod. This serves to prevent secondary hydriding, the cause of some spectacular cladding failures in conventional He-bonded fuel rods.

The LM-bonded hydride fuel rod is intended to replace oxide fuel in existing LWRs with no change in cladding dimensions. However, in the construction of the Generation III LWRs, the pitch of hydride fuel rods can be reduced, resulting in a smaller core and pressure vessel.

There are, however, several significant disadvantages of LM-bonded hydride fuel rods.

First, the uranium density of the hydride is only 40% that of oxide fuel. To maintain the same linear power, the U-235 enrichment must be increased by a factor of 2.5 – that is, to 10–12%. This not only incurs a nontrivial increase in the enrichment component of the fuel-fabrication cost, but requires a revision of the

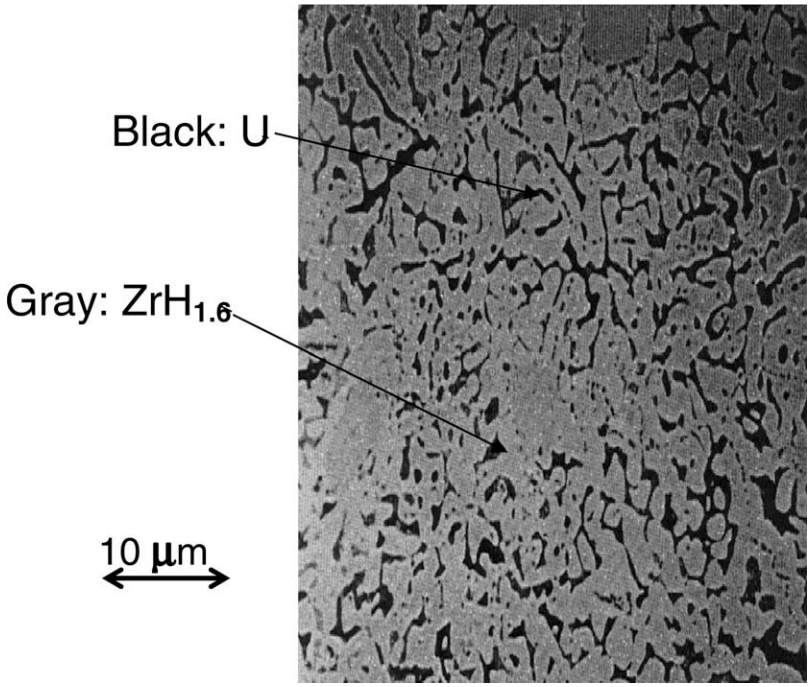

Fig. 8. Optical microscope picture of hydride fuel.

regulations governing maximum-allowable enrichment at fuel-fabrication facilities.

Second, very old data [8] suggest that the fission product volumetric swelling rate is three times larger than that of oxide fuel.

Third, the fabrication process is somewhat more complex than for helium-bonded fuel rods. Heating of the cladding tube is required to melt the charge of the Pb–Sn–Bi alloy and the fuel pellets must be pushed to the bottom in order to squeeze the liquid–metal into the fuel-cladding gap. However, fabrication of a full-size BWR fuel rod (4 m length of cladding with a 3 m stack of fuel pellets) has been demonstrated [7]. Fig. 9 shows a section of a finished rod from which the Zircaloy cladding has been removed. The liquid–metal covers the entire surface of the fuel, and in addition, penetrates pellet–pellet interfaces and cracks.

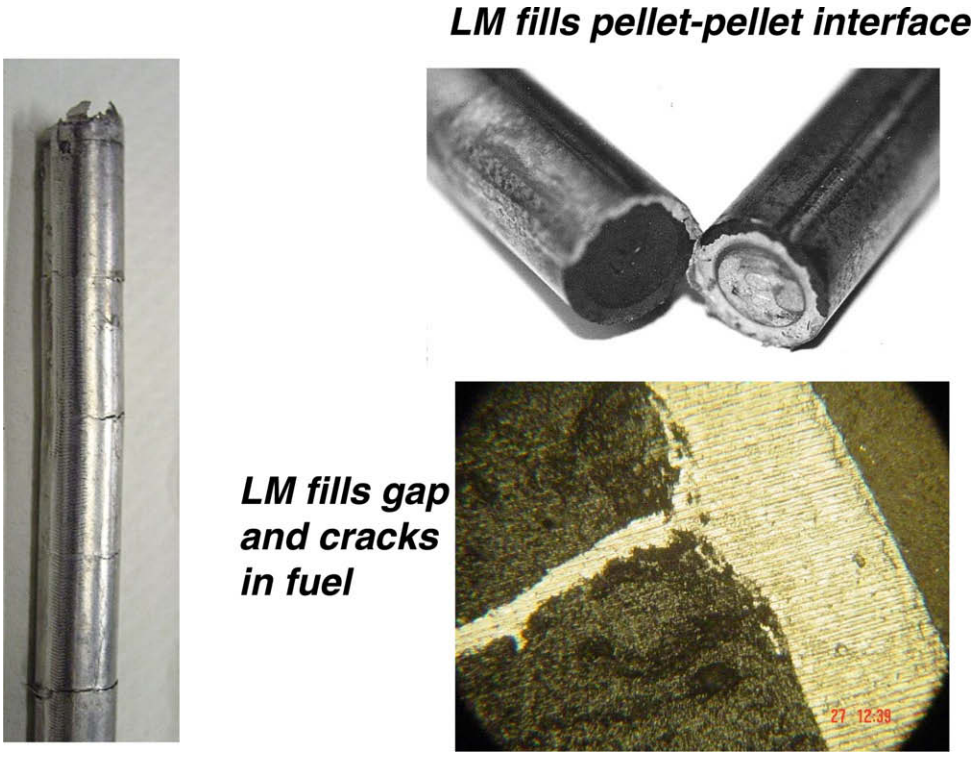

Fig. 9. Destructive examination of an as-fabricated LM-bonded fuel rod.

4. Oxide fuel chemistry

Fission of uranium produces an array of products that bind varying amounts of the oxygen released when a uranium atom fissions. This chemical effect profoundly influences the thermochemistry of the fuel.

The temperature and the oxygen-to-uranium molar ratio (O/U) of the fuel dictate the oxygen partial pressure, or the *oxygen potential*:

$$RT \ln p_{O_2} = F(O/U, T). \tag{1}$$

For $UO_{2\pm x}$ the function $F(O/U,T)$ is given, for example, in Ref. [9]. The oxygen potential determines the oxidation states of the fission products. Consequently, determination of the effect of burnup on the O/U of the fuel is the key problem to be worked out. To aid in this analysis, in Table 3 the fission products are collected into groups with approximately the same free energy of formation of the oxide.

MOX fuels utilize the mixed oxide $(U,Pu)O_{2-x}$, in which case the function F contains the U/Pu ratio as a variable. Considerable effort has gone into thermodynamic modeling of the U–Pu–O ternary system [10,11]. Even in the absence of Pu in the starting fuel, this element grows in with burnup; at a burnup of 60 MWd/kgU, the Pu fissions in initially pure, 20% enriched UO_2 constitute ~23% of the total. This effect, however, is neglected in the following analyses.

4.1. The oxidizing effect of fission in UO_2

A consequence of burnup is the dilution of uranium on the cation sublattice with oxygen-binding fission products. At a burnup of 60 MWd/kgU, the fissions per initial metal atom (FIMA) is 0.064. Approximately one-half of the fission products replace the vanished U in the fluorite structure of the fuel. Since there are two fission products per fission, the uranium ion concentration on the cation sublattice is reduced from 1 to ~0.94. These impurities affect the oxygen potential of the fuel in two ways. First, the replacement of U^{4+} by foreign ions that may be different in valence alters the interatomic forces, which affects all fuel properties, including the oxygen potential. Second, some of the original U^{4+} is promoted to U^{5+} or U^{6+} to maintain charge neutrality. Electrical neutrality can be perturbed either by introduction of ions of a valence other than 4+, for example La^{3+}, or by a sufficiently large oxygen pressure to result in insertion of oxygen interstitials into the fuel. In the latter case, UO_2 changes to UO_{2+x} and the free energy of formation of the oxide changes according to Ref. [17]:

$$\Delta G_f^o(UO_{2+x}) = \Delta G_f^o(UO_2) - \frac{1}{2}RT\int_0^x \ln p_{O_2}\, dx', \tag{2}$$

where $\Delta G_f^o(UO_2)$ is the free energy of formation of stoichiometric UO_2 and p_{O_2} is the stoichiometry-dependent equilibrium oxygen pressure over UO_{2+x} at temperature T (e.g. Eq. (1)).

4.2. The S factor

Fission causes uranium to disappear but does not affect oxygen. The latter can either be bound to reactive fission products (fp) or remain in the fuel associated with uranium. The oxygen-to-uranium ratio changes during fission according to:

$$\frac{O}{U} = \frac{2 - S \times \text{FIMA}}{1 - \text{FIMA}}, \tag{3}$$

S is the sum over all fission products of the atoms of oxygen bound to each:

$$S = \sum (z_i + q_i) A_i, \tag{4}$$

A_i is the number of oxygen atoms that fp_i binds (i.e. one-half of its oxidation state or valence). z_i is the fraction of a fission event that produces a species i that remains on the cation sublattice. At burnup FIMA, the fraction of the cation sites occupied by fp_i is $z_i \times$ FIMA. q_i is the analogous fraction of fissions that generate fp_i that reacts to form one or more of the ternary oxides shown in the last column of Table 3.

The fourth column in Table 3 gives ΔG_f^o at 1300 K for the reactions that form the generic fission product oxide fp_aO_b:

$$\frac{2a}{b}\text{fp} + O_2(1\,\text{atm}) = \frac{2}{b}\text{fp}_a\text{O}_b(s). \tag{5a}$$

The oxygen-binding number of fission product i is $A_i = (b/a)_i$. For comparison with ΔG_f^o of the fission product groups, the standard free energy of formation of UO_2 at 1300 K is $\Delta G_f^o(UO_2) = -830$ kJ/mole O_2. However, that of hyperstoichiometric urania is greater by the amount given by the second term in Eq. (2).

The dissolved portion of a particular fp group is a function of both the burnup and the prevailing oxygen potential. Dissolution of pure fp_aO_b onto the cation sublattice of the fuel is described by:

$$\frac{2}{b}\text{fp}_a\text{O}_b(s) = \frac{2a}{b}\text{fp}^{(2b/a)+}(\text{diss.}) + 2O^{2-}. \tag{5b}$$

Assuming ideal-solution behavior, the change in the chemical potential of an fp in this process is:

$$\Delta\mu = \frac{2a}{b}RT\ln(z \times \text{FIMA}).$$

Adding Eqs. (5a) and (5b) gives:

$$\frac{2a}{b}\text{fp} + O_2 = \frac{2a}{b}\text{fp}^{(2b/a)+}(\text{diss.}) + 2O^{2-}. \tag{5c}$$

If reaction (5c) is at equilibrium, the oxygen pressure is no longer 1 atm, and the overall free energy change is:

$$\Delta G_{6c} = \Delta G_{6a} + \Delta G_{6b} = 0,$$

Table 3
Oxygen binding by fission products.

Fission product	y_i	A_i	ΔG_F^o (1300 K) kj/mole O_2[b]	Solubility in UO_2, mole%[c]	Other oxides
Zr	0.30	2	−844	0.4 (<1473 K) 15 (1773)	$(Cs,Rb)_2ZrO_3$[f], $(Ba,Sr)ZrO_3$[f]
Mo[a]	0.24	2	−346	0.6	$(Cs,Rb)_2MO_4$[f,d] Sr_2MoO_4[e]
La…Y	0.55	1.5	−950	70–80 (La, Pr, Nd) 30(Y) Ce (miscible)	Many La[d]
Ba, Sr	0.16	1	−880	0.6 (Ba) 12 (Sr)[c]	$(Ba,Sr)UO_4$[f,d], $BaMoO_4$[d] Sr_2MoO_4[e]
Cs, Rb[a]	0.16	0.5	−170	<0.1	$(Cs,Rb)_2ZrO_3$[f], $(Cs,Rb)_2$ MoO_4[f,d] $(Cs,Rb)_2UO_4$[f,d]
Pd, Ru, Rh,Tc, Mo	0.26	0	–	0	–
Xe, Kr	0.30	0	–	0	–

[a] Part of these elements may exist as neutral atoms ($A_i = 0$).
[b] Of the oxide, from Ref. [12], using the code HSC (Ref. [16]).
[c] From Ref. [13].
[d] From Ref. [12] using HSC (Ref. [16]); in the presence of graphite.
[e] From Ref. [14].
[f] From Ref. [15].

or:

$$\Delta G_f^o - RT\ln p_{O_2} + \frac{2a}{b}RT\ln(z \times \mathrm{FIMA}) = 0,$$

rearranging yields the mass-action law for reaction (5c):

$$\exp\left(-\frac{\Delta G_f^o}{RT}\right) = \frac{(z \times \mathrm{FIMA})^{2a/b}}{p_{O_2}}. \quad (6)$$

This equation determines the dissolved fraction (z) of a particular fp as a function of the three global parameters T, FIMA and p_{O_2}. The latter depends upon the chemical states of all fission products and the O/M ratio of the fuel. If ΔG_f^o for a particular fp group is large and negative, the value of z calculated from Eq. (6) can exceed the nuclear yield of that group. Since this is not possible, reaction (5c) cannot be in equilibrium. Rather, all of that particular group is dissolved in the fuel. Such is the case for the rare-earth group.

The third possible chemical state of a fission product is elemental, for which the fraction is e_i. The sum of the three possible states is the nuclear yield:

$$y = z + q + e. \quad (7)$$

Each fission product group is characterized by the three numbers on the right of this equation. Another important characteristic of a fission product is its solubility in urania, which is shown in the fifth column of Table 3. A qualitative partitioning of the various fission-product groups is given in Table 4. The paired notation $<y$ $<y$ means that the element is split between the adjacent groups; ≈ 0 means that very little of the element is in the category; ≈ 1 means that nearly all of the element is in the category.

1. The rare-earth group dissolves completely in the fuel.
2. The oxides of the alkaline earths Ba and Sr have similar free energies of formation but the solubilities in the fuel are different (this is a cation-size effect). Essentially all Ba exists as a zirconate or uranate. The split of Sr between the fuel phase and one or more of the ternary oxide phases depends on the thermochemical state of the entire system (particularly the oxygen pressure).
3. ZrO_2 is stable with respect to urania but is nearly insoluble in the fuel phase. Consequently, Zr appears in one or more of the ternary oxides.
4. The oxide of Mo is quite unstable with respect to the fuel and exists either as an element alloyed with the noble metals or as a molybdate.
5. The alkali metals Cs and Rb are unstable with respect to the fuel but form quite stable zirconates, molybdates and uranates. There may be some Cs vapor in the fission-gas bubbles.
6. The noble metals form a separate phase in the fuel (see Fig. 7(b)). This phase may also contain Mo if the oxygen potential is sufficiently low.
7. The rare gases take no part in any solid phase.

The three groups that show low solubilities in the fuel nonetheless dissolve in the fuel at the beginning of irradiation. This is due to the limit FIMA $\to 0$ in Eq. (6), which permits large values of z. However, dissolution in the fuel is limited by the solubility of the element. With increasing burnup, the fuel oxide remains saturated with the fission product and the excess created by irradiation forms ternary oxides or the unoxidized element.

Fuel-performance computations intended to describe the chemical states of the fission products in irradiated UO_{2+x} or $(U,Pu)O_{2-x}$ invariably utilize one of the many codes that can handle large numbers of components.[2] These codes incorporate databases covering most of the compounds in Table 3 and many more. It is sufficient just to input the elements present and the code produces all of the possible compounds and their physical states. However, these results should be used with caution. The code HSC, for example yields La in six forms and three-phases: La, La_2O, LaO, La_2O_2, La_2O_3 and $La_3(MoO_4)_3$[12]. The default mode of the code is to mix all solids into a solid solution. If this is so, there is no reason to list all of the possible chemical states.

Table 4
Approximate partitioning of fission products in irradiated UO_2

Fission product group	z	q	e
Zr	≈ 0	≈ 1	0
Mo	≈ 0	$<y$	$<y$
La...Y	y	0	0
Ba	≈ 0	$\approx y$	0
Sr	$<y$	$<y$	0
Cs, Rb	0	≈ 1	≈ 0
Pd...Tc (Mo)	0	0	1
Xe, Kr	0	0	1

It is clear from the above discussion that the parameter S of Eq. (6) is not an immutable quantity. It is a function of temperature, oxygen potential and burnup. The thermochemistry of the fuel fission product solutions is sufficiently well-known to calculate the properties of the fuel phase with some confidence, the chemical properties of the zirconates, molybdates and uranates are much less firmly established. There is no agreement among the various fuel-performance codes as to which ternary oxides are important and their thermochemical properties. Until this aspect is improved, it is not possible to estimate the parameter S with any confidence.

However, this difficulty has not stopped fuel-performance analysts (including the present one) from doing their job. The method is simply to estimate S and hold it constant throughout irradiation, or allow it to change slowly with burnup. In either case, the behavior of the parameter S is simply an educated guess. In the following, a single value of S is selected and the consequences on fuel behavior calculated.

Whether the O/U ratio decreases with burnup depends on S. If this sum is less than 2, the O/U ratio increases with burnup, or the fuel becomes hyperstoichiometric. If $S > 2$, the fuel turns hypostochiometric. Forming this sum using Eq. (4) from the entries in Table 3 with all $z_i + q_i = y_i$ gives $S = 2.15$. According to Eq. (3), this should result in decreasing O/U with burnup. However, as noted in Table 4, Mo and the Cs, Rb combination may exist partially in the elemental state and not bind oxygen. If z and q for these fission products is zero, $S = 1.59$, and the fuel becomes progressively hyperstoichiometric with burnup. Where in the range $1.59 < S < 2.15$ the actual value lies depends on the details of the thermochemistry. The key parameter is the oxygen potential, which is involved in all of the element/oxide equilibria that determine the chemical states of the fission products. In most cases, the sum S is less than 2 because enough Mo exists as the element rather than as Mo^{4+} in ternary oxides where it binds oxygen [17]. In addition, the presence of non-fuel oxygen sinks such as Zircaloy cladding can significantly ameliorate or eliminate the increase of S with burnup.

5. Very-high-temperature reactor (VHTR)

Fig. 10 is a flow diagram of the VHTR listed in the last row in Table 2. A number of reactors of this type have been built and operated (e.g. the Fort Saint Vrain reactor in Colorado), but none are currently in use. The VHTR is explicitly designed to produce outlet coolant temperatures high enough to operate a hydrogen production plant. It may also generate electricity as a byproduct. It is a

[2] HSC[16] and FACTSAGE are two such codes.

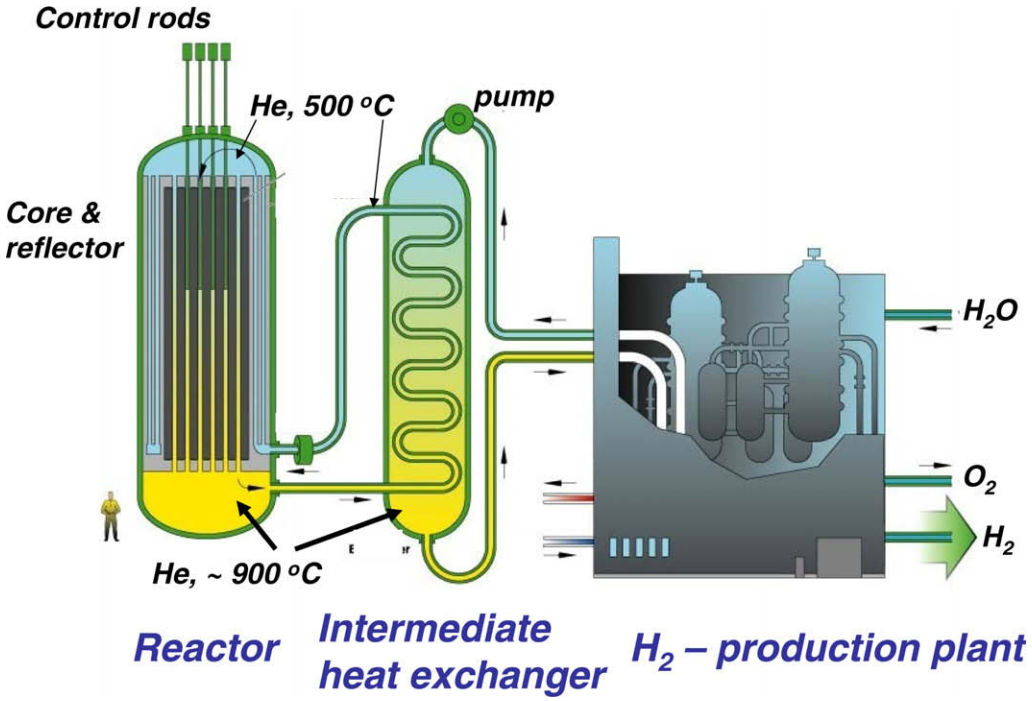

Fig. 10. The VHTR – a helium-cooled, graphite-moderated thermal-neutron reactor.

loop-type reactor, meaning that the coolant flows through the core and delivers energy to an external heat exchanger. In this sense, the VHTR is similar to LWRs. The helium coolant transfers energy to an intermediate heat exchanger, which may utilize either steam or helium as the secondary coolant. The primary helium from the reactor is not sent directly to the hydrogen plant in case the coolant is contaminated with fission products from leaking fuel.

Fig. 11 is a cross-section of the core of the VHTR. The shaded hexagons represent graphite blocks with axial holes, some for coolant flow and the rest for holding the small graphite cylinders containing fuel. The open hexagons in the drawing are graphite blocks without any penetrations. Their function is to return neutrons that leak from the core.

The heart of the VHTR is the small particle of fuel shown on the left of Fig. 12. These 1 mm-diameter spheres contain a *kernel* of fuel surrounded by three CVD layers of carbon and one layer of silicon carbide. Each layer has a distinct function, as indicated on the figure. The spheres are called tri-isotropic (TRISO)-layered particles; they were first developed in Germany.

The two types of graphite forms in which the fuel particles are dispersed are shown in the lower right of Fig. 12. One option is to embed the particles in a 5-cm long, 1.2-cm diameter graphite cylinder called a *compact*. These are then inserted into holes in the hexagonal graphite blocks that form the reactor core shown in Fig. 11. The other fuel form in which TRISO particles are contained are graphite spheres the size of tennis balls called *pebbles*. To form

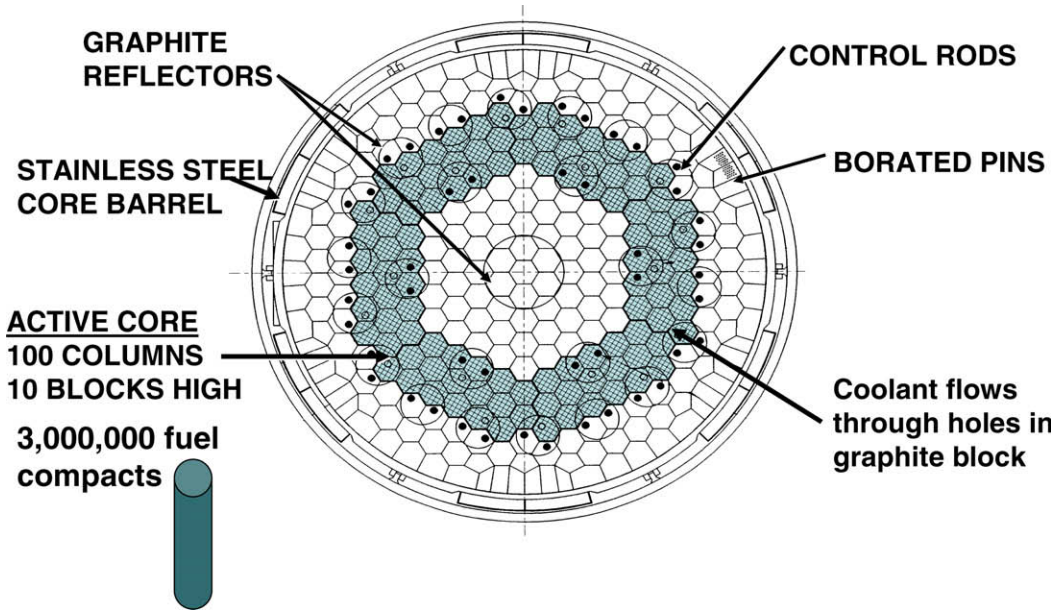

Fig. 11. Core configuration of the VHTR. Courtesy of D. Petti, Idaho National Laboratory.

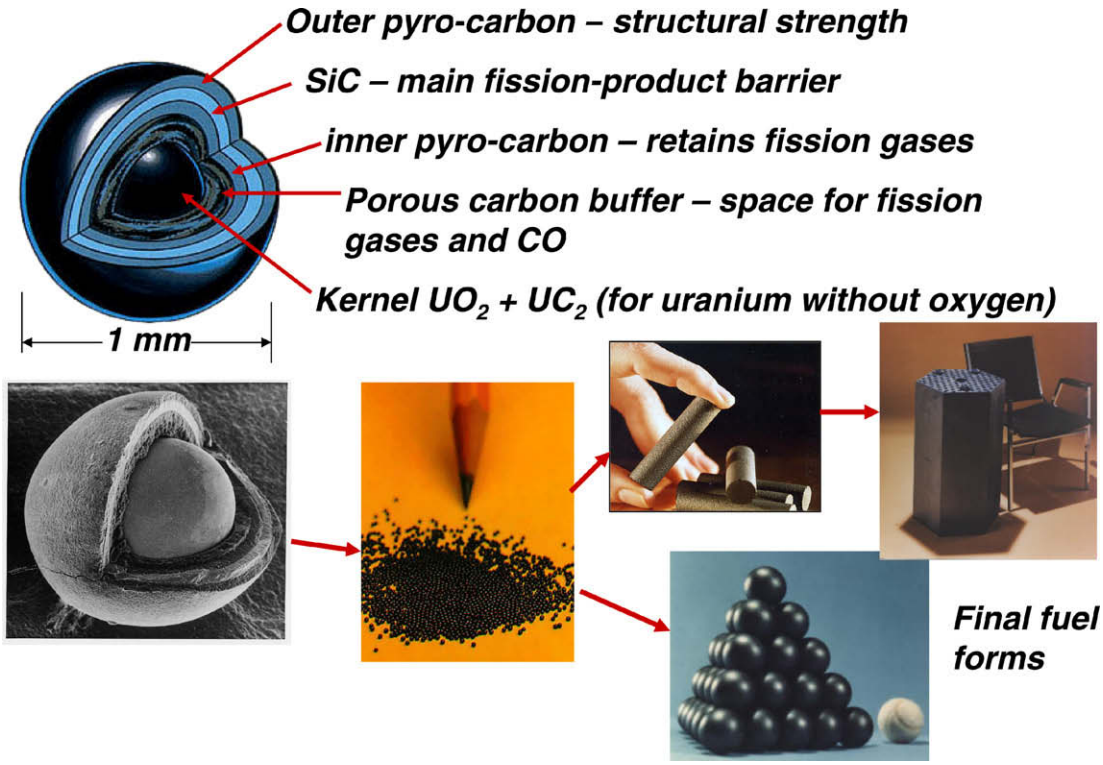

Fig. 12. TRISO fuel for the VHTR.

a reactor, these are loaded into a core barrel like popcorn in a box. The dimensions of the vessel are large enough for the contained pebbles to yield a critical mass. This so-called *pebble-bed reactor*, acronym THTR, was first constructed in Germany and operated from 1986 through 1989. A nearly identical reactor is currently under construction in South Africa. The VHTR in the US Generation IV program is an outgrowth of these programs, and will utilize compact-type fuels in the graphite neutron-moderator blocks shown in Fig. 11.

5.1. A practical TRISO particle

The only oxygen sink in a TRISO particle is the pure carbon of the buffer layer. Unfortunately, when this oxidizes, the gas produced (CO) contributes to the internal pressure in the particle. In addition, a portion of the oxygen not bound to fission products remains in the fuel, thereby converting UO_2 to UO_{2+x}. This simplest of particle fuels is analyzed in this section.

A workable fuel for a VHTR differs from the isolated UO_2 described in Section 4 in two ways, both related to the buffer layer of carbon surrounding the kernel: (i) a restricted void space is available to accommodate gases; (ii) the kernel is in contact with carbon.

As UO_{2+x} is formed during burnup, it is reduced by the reaction:

$$UO_{2+x} + xC \rightarrow UO_2 + xCO. \quad (8)$$

The carbon monoxide produced by this reaction accumulates in the porosity of the buffer layer The CO pressure in this volume can attain large values if the fuel is pure UO_2 and, along with the pressure contributed by the released fission gases, can compromise the integrity of the pyrocarbon layers (Fig. 13(a)).

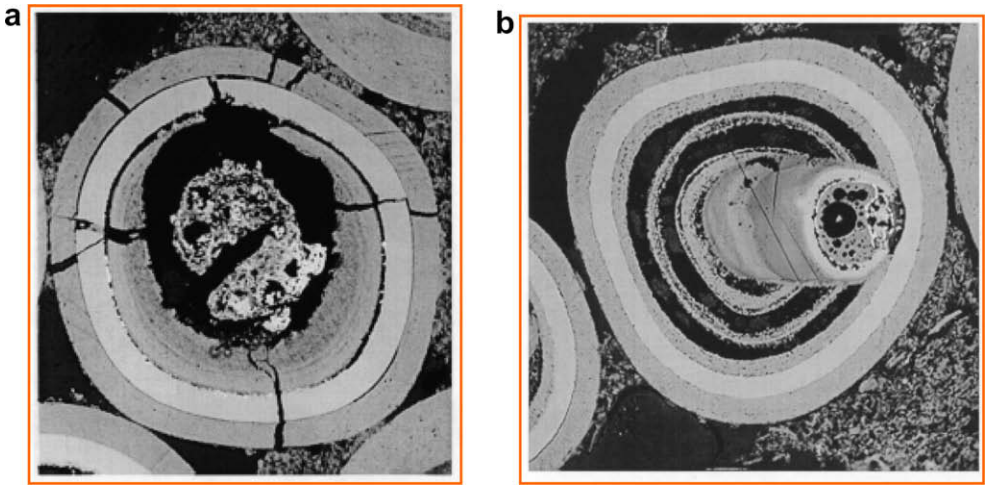

Fig. 13. TRISO kernels after irradiation: (a) mechanical failure by fission gas and CO pressure; (b) kernel migration by the CO mechanism.

Eq. (8) is not an equilibrium reaction; rather, it is meant solely to indicate the role of carbon in maintaining the stoichiometry of the fuel, but at the expense of producing CO.

The sequence of steps in modeling the thermochemistry of an initially-stoichiometric UO_2 kernel is sketched in Fig. 14. N initial moles of UO_2 with burnup given by FIMA results in reduction of the quantity of uranium to $(1 - \text{FIMA}) \times N$ but does not affect the oxygen. The quantity of oxygen bound chemically to fission products is $S \times \text{FIMA} \times N$. Because $S < 2$, the quantity of oxygen not attached to fission products is $(2 - S \times \text{FIMA}) \times N$. This excess O is partitioned between the fuel and the gas-phase. The partitioning is described by $\boldsymbol{f}$, which is defined as the fraction of the available oxygen that remains with the fuel (over and above that combined with reactive fission products). The fraction $1 - \boldsymbol{f}$, which is termed 'free' oxygen in Fig. 14, escapes to the buffer void volume where it reacts to form CO.

Carbon monoxide is produced from the 'free' oxygen by the reaction $2C + O_2 = 2CO$, the equilibrium constant of which is:

$$K = p_{CO}^2 / p_{O_2}. \tag{9}$$

The standard free energy change is:

$$\Delta G^o = -224000 - 176 \times T \text{ J/mole}$$

The equilibrium constant $K = \exp(-\Delta G^o/RT)$ is very large, so essentially all of the gas-phase oxygen is present as CO at a pressure given by the ideal gas law:

$$p_{CO} = (1 - f) \times (2 - S \times \text{FIMA}) \times (\text{NRT}/V_{\text{buffer}}). \tag{10}$$

The O/U ratio given by:

$$\frac{O}{U} = \frac{f \times (2 - S \times \text{FIMA})}{1 - \text{FIMA}}. \tag{11}$$

This result was derived earlier by Arai [18].

The fraction $\boldsymbol{f}$ is determined as follows. Eq. (10) is inserted into Eq. (9) to determine p_{O_2}, which is then substituted into Eq. (1) and the result solved (numerically) for $\boldsymbol{f}$. With $\boldsymbol{f}$ so determined, O/U and p_{CO} are calculated from Eqs. (10) and (11). Finally, the partial pressure of O_2 in the buffer void space is given by Eq. (1).

Example: Kernel: pure UO_2 initially; $S = 1.7$ (arbitrary choice) $T = 1400$ K FIMA = 0.5. The following are typical values for the TRISO particle: Kernel diameter = 350 μm; kernel density = 10.4 g/cm^3 → $N = 6.5 \times 10^{-7}$ moles UO_2 buffer thickness = 100 μm; buffer porosity = 0.5 → $V_{\text{buffer}} = 3.2 \times 10^{-5}$ cm^3.

$\text{NRT}/V_{\text{buffer}} = 2.3 \times 10^3$ atm; $2 - S \times \text{FIMA} = 1.15$; In Eq. (9), $K = 3.2 \times 10^{17}$. For the quantities in this example, Eqs. (10) and (11) reduce to:

$$p_{CO} = 2.6 \times 10^3 (1 - \boldsymbol{f}), \tag{10a}$$

and

$$x = 2.3 \times \boldsymbol{f} - 2. \tag{11a}$$

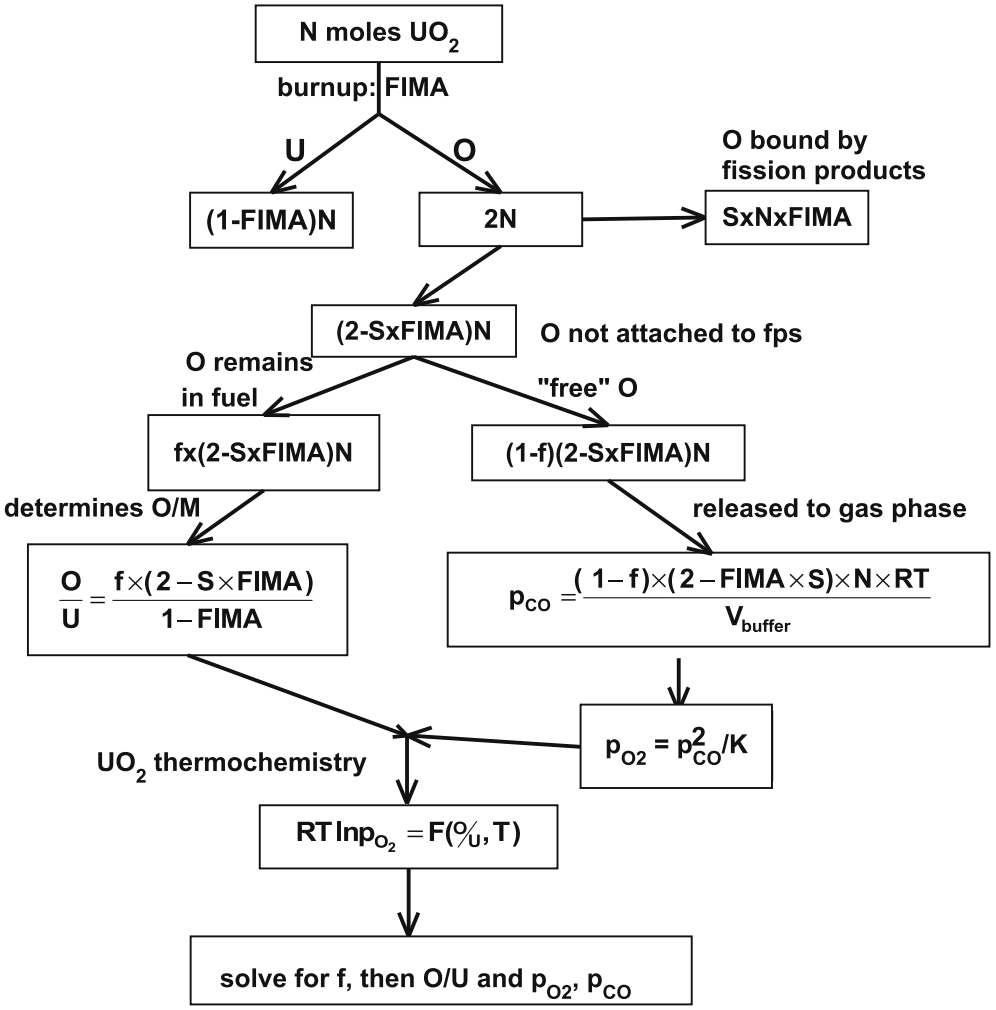

Fig. 14. Irradiation effect on the O_2 and CO partial pressures and the O/U ratio of a UO_2 fuel kernel with loss of oxygen to a gas space.

The oxygen partial pressure based on the CO pressure is obtained from Eq. (9) using Eq. (10a):

$$\ln p_{O_2} = -24.6 + 2 \times \ln(1 - \boldsymbol{f}). \tag{9a}$$

The oxygen partial pressure as a function of hyperstoichiometry x is obtained from Ref. [9] (or by one of many more advanced thermochemical methods). For $T = 1400$ K, Eq. (23) of Ref. [9] is:

$$\ln p_{O_2} = -5.2 + 4 \ln \left[\frac{2x(1-2x)}{(1-4x)^2} \right]. \tag{12}$$

The $\ln p_{O_2}$ values from Eqs. (9a) and (12) are equal for $\boldsymbol{f} = 0.870$, which, by Eq. (11a), corresponds to $UO_{2.001}$. The oxygen partial pressure is 5×10^{-13} atm and $p_{CO} = 338$ atm. Such a large CO pressure in the particle is untenable.

5.2. Influence of UC_2

In the US VHTR, the fuel is a 3:1 ratio of UO_2:UC_2. The role of the UC_2 is straightforward: as oxygen is liberated from the fuel, UC_2 reduces it back to UO_{2+x} according to[3]:

$$O_2(\text{“free”}) + UC_2 \rightarrow UO_2 + 2C. \tag{13}$$

Because this sequence does not release CO, it is more desirable than the reaction that would occur in the absence of UC_2 (Eq. (8)).

To thermodynamically assess the effect of the UC_2 component of the fuel, one of the following equilibria needs to be considered:

$$UO_{2+x} + (4+x)C = UC_2 + (2+x)CO, \tag{14a}$$

or

$$2UO_{2+x} + (7+2x)C = U_2C_3 + 2(2+x)CO. \tag{14b}$$

Whether the dicarbide or the sesquicarbide is present depends upon temperature [19].

The mass-action law for reaction (14a), (14b) provides a relation between x and p_{CO}. For reaction (14a), for example

$$p_{CO}^{2+x} = \exp(-\Delta G_{14a}/RT), \tag{15}$$

where

$$\Delta G^o_{14a} = (2+x)g^o_{CO} + g^o_{UC_2} - g^o_{UO_{2+x}} - (4+x)g^o_C \tag{16a}$$

where g_i^o is the standard (i.e. at 1 atm) free energy of pure species i at temperature T. The thermochemical information available is for the reaction with $x = 0$:

$$\Delta G^o_{14a,x=0} = 2g^o_{CO} + g^o_{UC_2} - g^o_{UO_2} - 4g^o_C, \tag{16b}$$

for which [19]:

$$\Delta G^o_{14a,x=0} = 758 - 350(T/10^3)\ \text{kJ/mole} \tag{17}$$

Subtracting Eq. (16b) from (16a) gives:

$$\Delta G^o_{14a} = \Delta G^o_{14a,x=0} + x(g^o_{CO} - g^o_C) - (g^o_{UO_{2+x}} - g^o_{UO_2}).$$

Since the last term is given by Eq. (2)

$$\Delta G^o_{14a} = \Delta G^o_{14a,x=0} + x(g^o_{CO} - g^o_C) + frac12RT \int_0^x \ln p_{O_2}\, dx'. \tag{18}$$

The calculation proceeds as follows:

- Eq. (9) provides a relation between p_{CO} and p_{O_2}.
- Eq. (1) provides a relation between p_{O_2} and $O/U = 2 + x$.
- Eq. (15), in conjunction with Eq. (18), provides a relation between x and p_{CO}.

These three equations need to be solved simultaneously for the three unknowns.

The analysis described above is too simplistic for obtaining accurate results. A more reliable calculation would need to account for the change of the oxygen-binding parameter S (Eq. (4)) with burnup. This effect is due to the continued introduction of fission products and the change in the oxygen pressure with burnup.

Using Eq. (1) to calculate the oxygen potential considers only the effect of dissolved fission-product valences. The sole effect dissolved rare-earth fps with +3 valence is assumed to be to promote an equivalent number of U^{4+} to U^{5+}. The same uranium valence promotion can be achieved by adding oxygen interstitials to pure UO_2. For example, a fraction x_{RE} of RE^{3+} on the cation lattice is equivalent to UO_{2+x} with $x = 1/2\ x_{RE}$. Eq. (1) can then be used to calculate the oxygen potential. This approach, which is termed the *valence-control rule*, is only approximate. It correctly predicts an increase of the oxygen potential of urania doped with La^{3+} and a decrease if urania is doped with Nb^{5+}. However, the rule is not sufficiently accurate for quantitative analysis [20].

5.3. An approximate example

The necessity of solving the three simultaneous equations given above can be avoided by assuming $x = 0$ throughout the irradiation. With this simplification, Eqs. (15) and (17) yield $p_{CO} = 1 \times 10^{-5}$ atm at 1400 K. Even without the detailed calculation, the CO pressure remains very small as long as UC_2 is present.

The $x = 0$ approximation can also be utilized to determine whether the UC_2 component is consumed by the oxygen released by fission of U in the oxide phase. The fuel initially consists of N moles of UO_2 and M moles of UC_2. After burnup FIMA, the moles of O tied to the $(1 - \text{FIMA}) \times N$ moles of U remaining is $2(1 - \text{FIMA}) \times N$. In addition, $S \times \text{FIMA} \times N$ moles of O are bound to the fission products in the oxide, leaving

$$2N - 2N \times (1 - \text{FIMA}) - S \times \text{FIMA} \times N$$
$$= 2\left(1 - \frac{1}{2}S\right) \times \text{FIMA} \times N \text{ moles of O}$$

free to interact with the UC_2 component of the fuel, which now consists of $(1 - \text{FIMA}) \times M$ moles of U and $\text{FIMA} \times M$ moles of fission product, some of which are present as carbides. If all of the fission product carbides must be converted to oxides before UC_2 can react to form UO_2, the fission product carbides would consume $S \times \text{FIMA} \times M$ moles of O. Whether this is greater or less than the amount of O available from the fuel depends on the initial oxide to carbide ratio N/M. If all available O were consumed by oxidizing fission-product carbides, the fraction converted from carbide to oxide would be:

$$\frac{2 - S}{S}\frac{N}{M}$$

For the fission-product-oxygen-binding factor $S = 1.7$ and $N/M = 3$, as in the US VHTR, just over one-half of the fission product carbides can be converted to oxides but none of the UC_2 is chemically affected.

Homan et al. [21] have also analyzed the interconversion of fission-product oxides to the corresponding carbides in mixed UO_2/UC_2 fuel.

5.4. Kernel migration

Mechanical rupture of the structural pyrocarbon layers of the particle (see Fig. 13(a)) is not the only deleterious effect of CO on TRISO particle performance. Another is kernel ‘migration’, a

[3] Eq. (13) is not an equilibrium reaction – it merely indicates the direction of the conversions that take place as oxygen is liberated with burnup.

phenomenon shown in Fig. 13(b) that appears to cause the kernel initially at the center of the particle to move off-center. If the kernel 'moves' sufficiently far off-center as to touch the SiC layer in Fig. 12, rupture of the latter can occur with concomitant loss of fission products.

Actually, the kernel does not move; the rest of the particle does. Fig. 15 illustrates the mechanism. A temperature gradient through the compacts is needed in order to transfer heat from the center to the edge, whence it ultimately reaches a coolant channel. As a corollary, each particle sustains a temperature gradient, and it is this nonuniformity that causes material movement.

The cause is the temperature dependence of the equilibrium constant for the reaction:

$$2CO = CO_2 + C, \tag{19}$$

$$\text{for which :} \quad K = p_{CO_2}/p_{CO}^2. \tag{20}$$

Being an exothermic reaction, K decreases with increasing temperature. Consequently, the hot side of the particle has a lower CO_2/CO ratio than the cold side, thereby driving a flux of CO_2 up the temperature gradient. Upon arriving at the hot side, CO_2 reacts with C according to reaction (19) in order to maintain the equilibrium partial pressures. At the cold side, the CO moving from hot-to-cold decomposes and deposits carbon. The net result is removal of carbon on the hot side and deposition of carbon at the cold side. This transfer of carbon gives the visual impression of kernel migration. Carbon is first removed from the buffer layer at the hot side, then from the inner pyrocarbon layer. The kernel eventually touches the silicon carbide layer.

Both the mechanical stress and the kernel migration effects are due to a high CO pressure in the buffer volume.

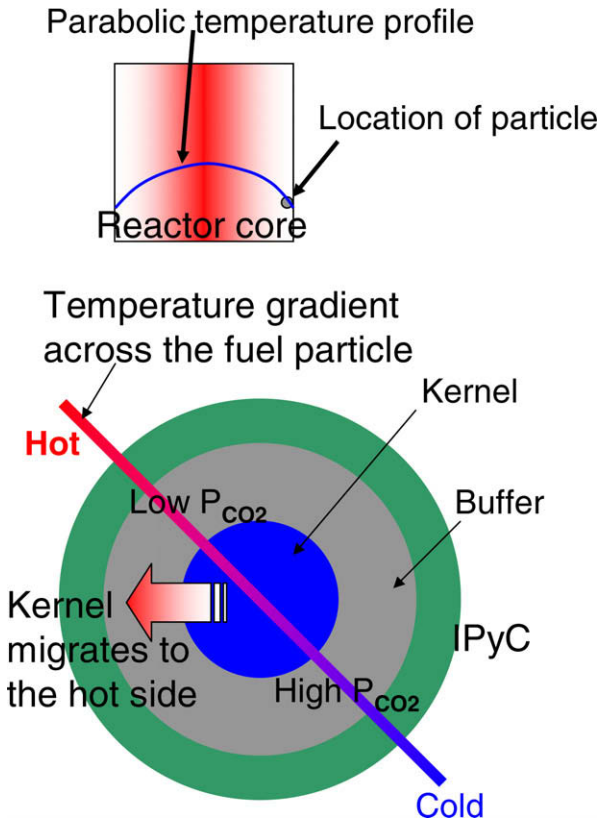

Fig. 15. Migration of the kernel in a temperature gradient.

6. Reprocessing of particle fuel

6.1. The purex process

At present, the only large-scale scheme for reprocessing spent nuclear fuel to separate fission products, plutonium, and uranium is the PUREX (short for plutonium extraction) process. This is an aqueous solvent extraction method that was used to remove weapons-grade Pu from the uranium slugs irradiated in the Hanford production reactors. This process is also used in the UK and France (and soon in Japan); the separated plutonium is mixed with depleted uranium to form MOX fuel for LWRs.

Briefly, the PUREX process involves the following steps:

1. Dissolving the uranium in nitric acid. This leaves U as U^{6+} and Pu as Pu^{4+}.
2. Extracting U^{6+} and Pu^{4+} nitrates from the aqueous phase by contacting with a solvent containing the complexing molecule tributyl phosphate (TBP) in a diluent such as kerosene. The fission products and the minor actinides are not extracted because they are not complexed by TBP.
3. Scrubbing (stripping) the U and Pu from the organic phase to an aqueous nitric acid phase.
4. Reducing Pu^{4+} to inextractable Pu^{3+} by, for example, passing the solution over a bed of iron filings.
5. Using the aqueous solution of U^{6+} and Pu^{3+} as the feed to a second solvent extraction to recover separate highly-purified U and Pu streams.

6.2. Recent changes in reprocessing requirements

Recently-changed requirements for reprocessing have rendered the PUREX process obsolete:

1. For proliferation reasons, Pu can no longer be recovered in a pure state.
2. Pu, along with the minor actinides Np, Am and Cm, must be burned by subsequent reactor irradiation. This step removes the long-lived transuranics from entering the waste repository, where they would constitute the major portion of the radioactivity (and heat load) at very long storage times.
3. Burning and/or separation of the minor actinides and separation of the alkaline earth fission products barium and strontium permit a denser loading of waste in a repository than is possible with unreprocessed spent fuel. The reasons for this are temperature limitations at various times and positions in the repository. Fig. 16 shows the relative waste-packing density compared unreprocessed spent fuel [13]. The limiting temperatures are 200 °C at the drift wall and 96 °C half way between drifts.[4] The variables are the fraction of the minor actinides on one axis and Cs/Sr on the other axis remaining in the waste following reprocessing. It can be seen that if all but 0.1% of these groups are removed, the drifts can be loaded with 225 times as much waste as unreprocessed spent fuel elements. The heights of the columns are fixed by reaching limiting temperatures at various times. The limits are:

1. Drift wall at time of placement of the waste in the drift (25 years).
2. Drift wall at time of closure of the drift (100 years).
3. Mid-drift temperature (>1600 years).

[4] A drift is a large hole in the rock of a repository in which high-level wastes are stored.

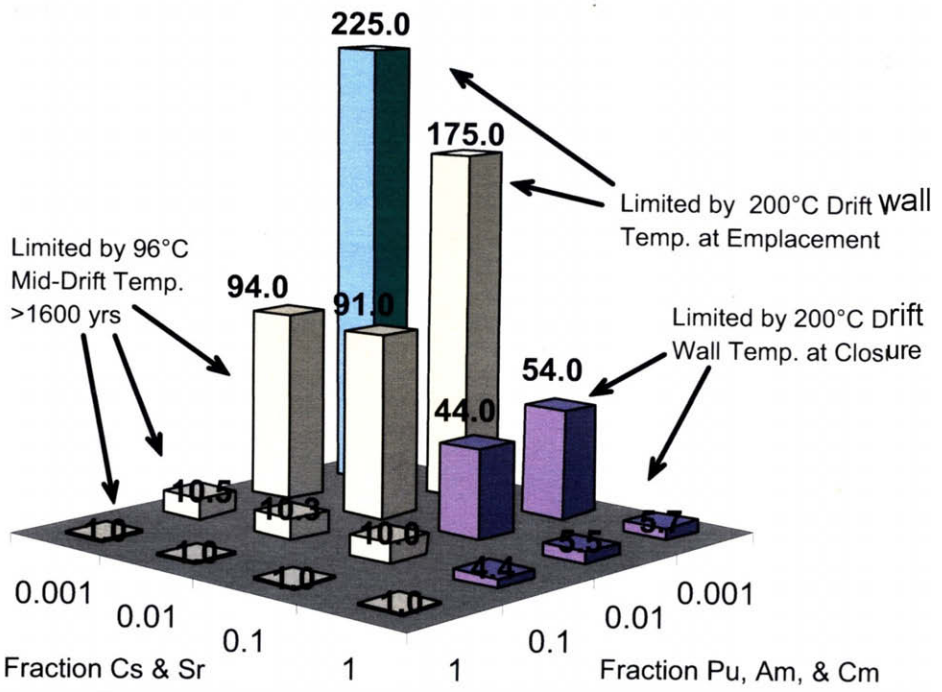

Fig. 16. Relative drift loading as a function of separation efficiencies of the minor actinides and the alkaline earths [22].

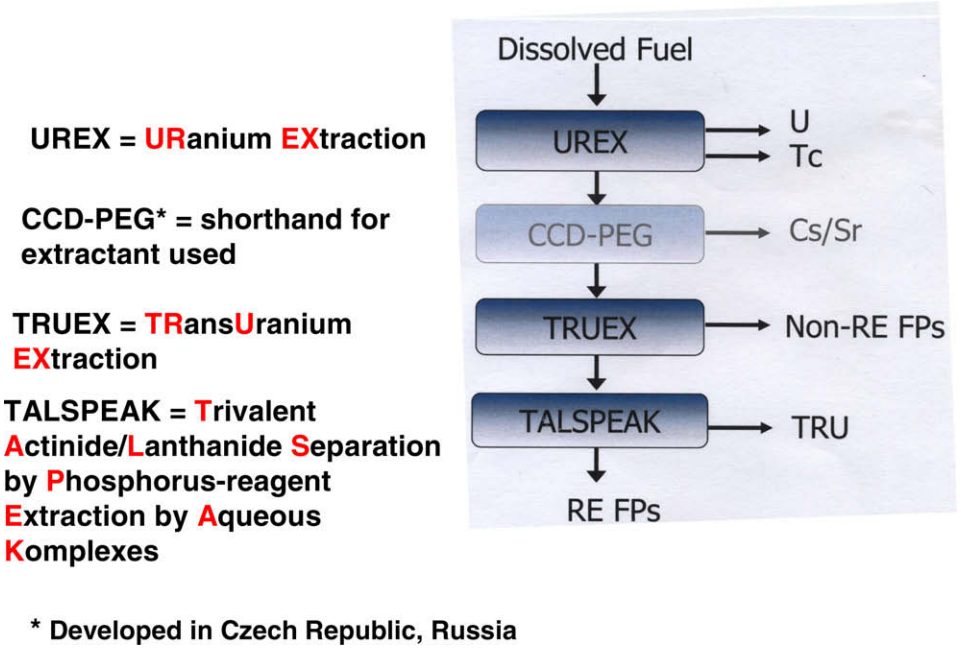

Fig. 17. Suite of extraction steps in the UREX-1a reprocessing method.

Fig. 16 shows that removal of the TRU nuclides is important in limit No. 3 while the short-term limits 1 and 2 are controlled by removal of Cs and Sr. This graph demonstrates the necessity of removing these two groups of elements from the spent fuel if the repository such as Yucca Mountain is to be capable of storing high-level waste for many years. If the prohibition on reprocessing in the US continues and all of the waste currently stored on reactor sites were transferred as spent fuel to Yucca Mountain when it opens, the repository would be filled to capacity and have to shut down immediately.

6.3. The UREX+1a suite of extractions

Fig. 17 shows a much more complicated 'suite' of extraction processes designed to remove the shortcomings of the old PUREX process.

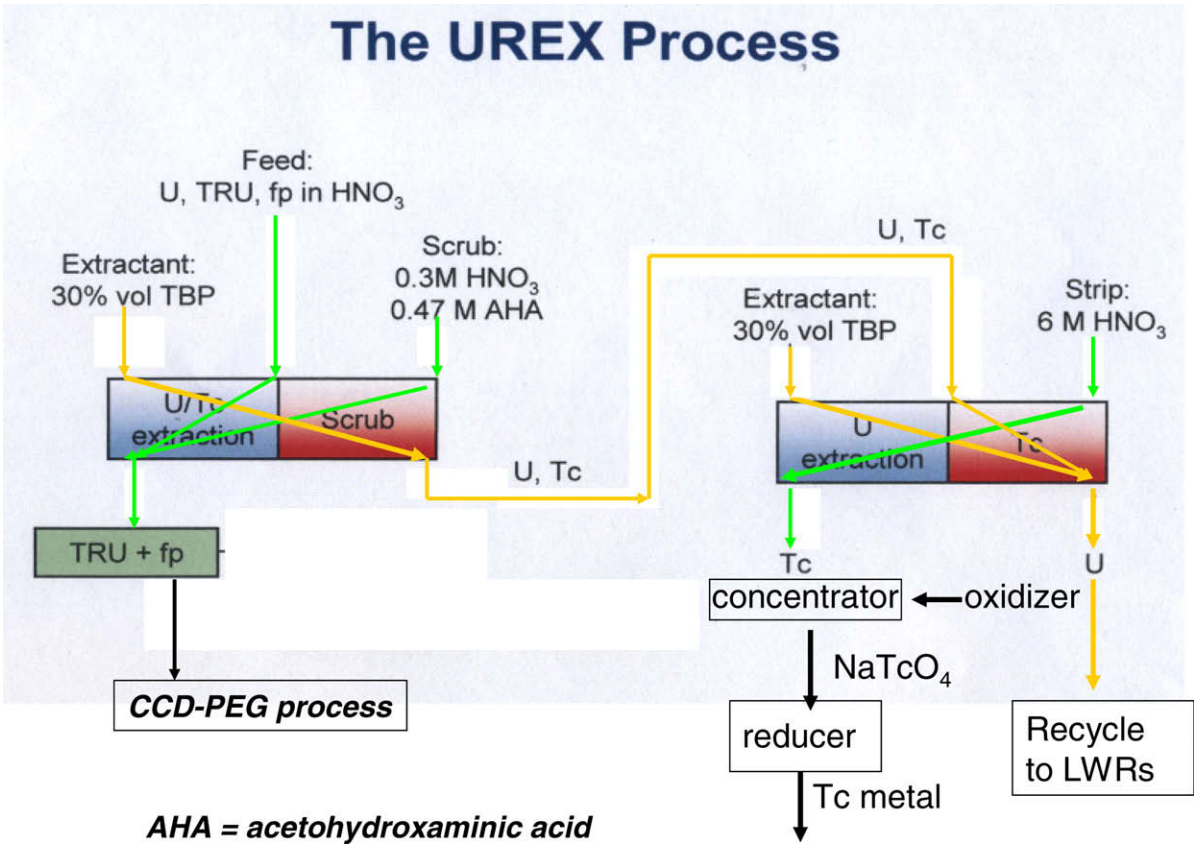

Fig. 18. The UREX process.

The first step, called UREX (for URanium EXtraction), separates uranium and technetium together from the spent fuel. A subsequent step (not shown) separates U and Tc from each other. The uranium is re-enriched with U-235 or Pu-239 and recycled to LWRs. The recovered Tc is alloyed with the Zircaloy cladding material and removed as waste.

The second step is called CCD-PEG after the extractant used removes cesium and strontium from the aqueous stream issuing from the UREX process.

The third process, TRUEX, removes all but the trivalent ions (rare-earths and the minor actinides) from the waste.

The last process, TALSPEAK, is intended to perform the difficult separation of the minor actinides (TRU) from the lanthanides.

Fig. 18 shows the details of the UREX process. Yellow arrows represent organic phase flows; green arrows are aqueous flows.[5] The dissolved spent fuel is fed to the middle of a solvent extraction device (either a column or a series of centrifugal separators) that removes U and Tc to the organic extractant but leaves the TRU along with all fission products in the aqueous phase. The scrub section is intended to remove unwanted nuclides from the organic phase with a very specialized organic chemical (AHA).

The organic product containing U and Tc is the feed to a second column using the same extractant but a different scrub (strip) solution. Uranium remains in the organic phase but technetium is removed to the aqueous phase, from which it is eventually converted to metal.

Table 5 shows the subsequent steps illustrated in Fig. 17.

The CCD-PEG process separates cesium and strontium (CCD for Cs and PEG for Sr). The TRUEX process removes the non-rare-earth fission products for disposal and delivers the stream containing the minor actinides and the rare-earth fission products to the final extraction, called TALSPEAK. The rare-earth fission products are sent to a geologic repository after vitrification and the minor actinides (and Pu) are recycled to a reactor capable of fissioning them, thus removing them from the waste stream.

The series of separations shown in Fig. 17 are part of the Global Nuclear Energy Partnership (GNEP) program in which many countries participate. However, none of the processes have reached the pilot-plant scale of development.

Table 5
Components of the UREX-1a suite of extractions.

PROCESS	AQUEOUS FEED	EXTRACT. (DILUENT)	SCRUB	RAFFI-NATE	PRODUCT
UREX	Spent fuel, fp w/o Xe,I	TBP[a] (dodecane)	Dilute HNO_3 AHA[i]	TRU, fp in HNO_3	U, Tc In TBP
CCD-PEG	TRU, fp in HNO_3	CCD[b],PEG[c] (FS-13[e])	2 M HNO_3	TRU, fp in HNO_3	Cs, Sr In CCD-PEG
TRUEX	TRU, fp in HNO_3	TBP, CMPO[d] (dodecane)	HNO_3	non-RE[f] fp	TRU, RE fp in aqueous
TALSPEAK	TRU, RE fp	HDEHP[g] (dodecane)	Lactic acid, DTPA[h]	TRU	RE fp in aqueous

[a] Tributyl phosphate.
[b] Cobalt dicarbollide (for Cs).
[c] Polyethylene glycol (for Sr).
[d] n-Octyl-diphenyl-di-isobutyl-carbamoyl-methyl-phosphine oxide.
[e] Phenyltrifluorosulfone.
[f] Rare-earth fission products.
[g] Di(2-ethylhexyl) phosphoric acid.
[h] Diethylenetriamine-pentaacetic acid.
[i] Acetohydroxaminic acid.

[5] For interpretation of color in Fig. 18, the reader is referred to the web version of this article.

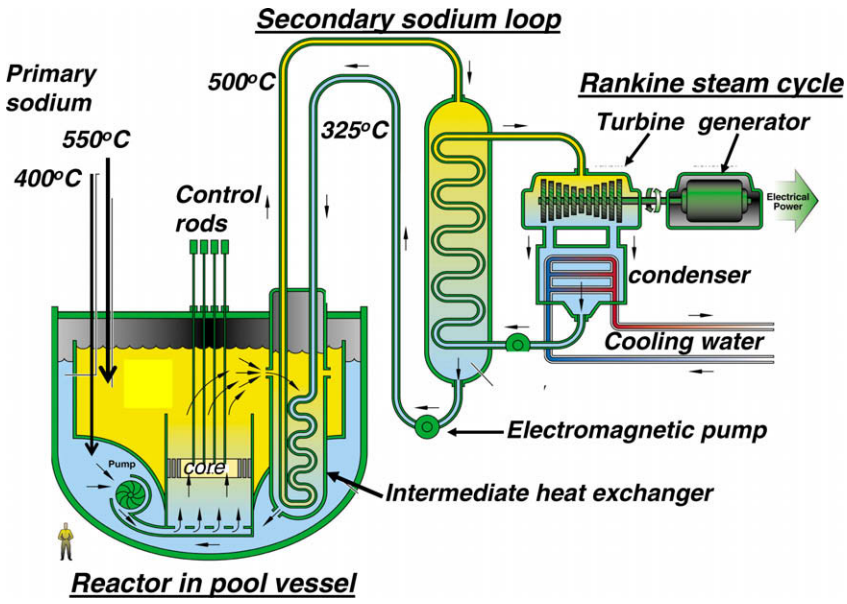

Fig. 19. Pool-type sodium fast reactor (SFR).

7. The sodium fast reactor (SFR)

Fig. 19 shows the power-generation plant driven by a sodium-cooled fast reactor. As the name implies, the coolant is liquid sodium. Contrary to the loop-type system of the VHTR (Fig. 10), the heat exchanger that transfers the energy extracted from the core by the primary sodium to a secondary sodium circuit is located in a pool of liquid sodium. The electromagnetic pump pushes sodium coolant up through the core and into a large inside section of the pool where the temperature is about 550 °C. The primary sodium exiting the shell side of the intermediate heat exchanger is pumped into the core. The heated secondary sodium drives a second heat exchanger with water in the tube side. This drives an ordinary Rankine cycle to produce electricity. However, an equally-important function of the SFR is to burn the minor actinides and plutonium.

The fuel assembly for the sodium fast reactor is shown in Fig. 20. The hexagonal assemblies, each holding 270 fuel pins, are set into a lower grid plate. They are fixed at the upper part by two spacer pads, which is where each assembly contacts the six surrounding assemblies.

Fig. 21 depicts the fuel pin, which is what a fuel rod or fuel element is called in the fast reactor trade. The fuel pin is smaller than the fuel element of a LWR, being only 6.5 mm in diameter. Its cladding is made of a ferritic steel HT9 because this type of steel is much more resistant to void swelling than the austenitic steels such as 316.[6] HT9 is especially hardened to give it strength normally lacking in ferritic steels.

The fuel is an alloy of depleted uranium with 20% of recycled TRU and 10% zirconium. The last of these elements raises the liquidus temperature and increases the resistance to fuel-cladding interaction. A noteworthy feature of the SFR fuel pin is the huge (compared to LWR) fuel-cladding gap, the reason for which will be reviewed later. Because of the large gap, the sodium bond is essential for avoiding excessively high fuel temperatures.

[6] Zircaloy, the cladding of LWRs, is not used in fast reactors because low thermal-neutron absorption of Zr is of no use in the high-energy neutron spectrum of the SFR. It is also much more expensive than steel.

The fuel pin is rather short – less than 2 m long. About 1 m contains fuel slugs with the sodium bond in the fuel-cladding gap. An equally long section is devoted to a plenum to receive released fission gases without overpressurizing the cladding wall. The other noteworthy feature of the fuel pin is the wire wrapping. This serves two purposes. The first is to separate fuel pins. The second is to induce a swirl in the upflowing sodium coolant to improve convective heat transfer.

7.1. Irradiation effects on metal fuel

Fig. 22 shows photomicrographs of cross-sections of the fuel pin before and after irradiation. The Zr component of the as-fabricated fuel forms a separate phase in the U–Pu matrix.

After irradiation, a number of profound changes take place. First, there is extensive separation of the elemental components. There are usually three distinct radial zones, but in this case only the low-melting central phase, which is close to the eutectic composition that melts at about 700 °C, is formed. Except for the outer surface, the outer annulus of the fuel does not exhibit significant changes. The right-hand photomicrograph of Fig. 22 reveals extensive fuel-cladding interaction, with the rare-earth fission products and plutonium liquefying the cladding by forming an alloy with iron. The figure shows that the initial 600 μm radial gap has completely closed. This occurs rather early during irradiation because swelling of the fuel due to fission-gas bubbles is large.

Fig. 23 shows the close relation between swelling and fission gas release in metal fuel. Fission gas precipitates into large bubbles (black areas) very early in irradiation. If the fuel-cladding gap is too small, the swelling fuel exerts an unacceptably-large stress on the cladding. However, at about 33% swelling, the gas bubbles interlink and vent their contents to the plenum. Thereafter, the swelling rate diminishes drastically (right-hand plot in Fig. 23). The design compromise is to allow for a gap sufficiently large so that bubble interlinkage and closure of the gap occur simultaneously. This requirement is fulfilled with an initial gap thickness if the neighborhood of 600 μm. With this stratagem, burnups up to 75% FIMA are attainable, and essentially complete burnup of the minor actinides and plutonium is achieved.

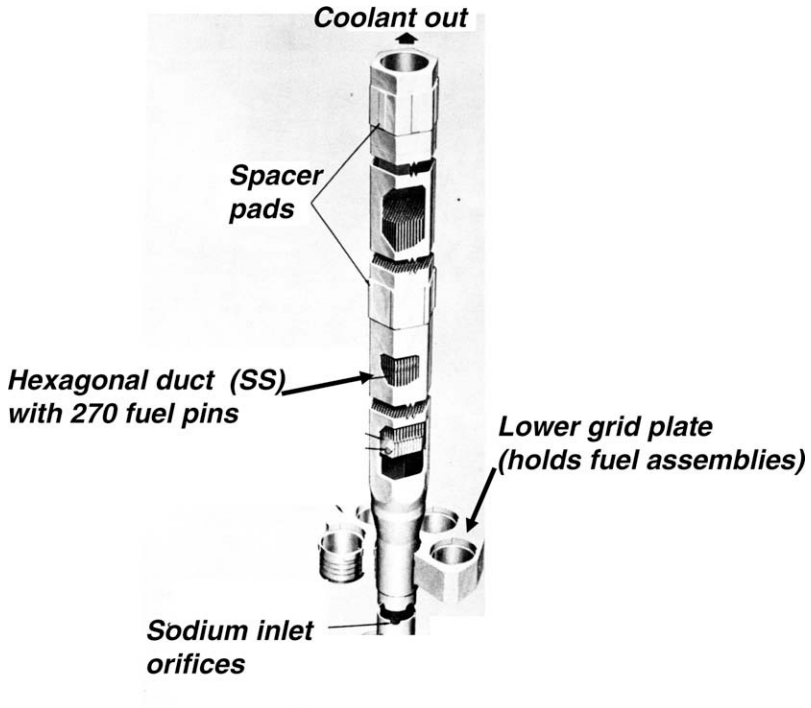

Fig. 20. Sodium fast reactor fuel assembly.

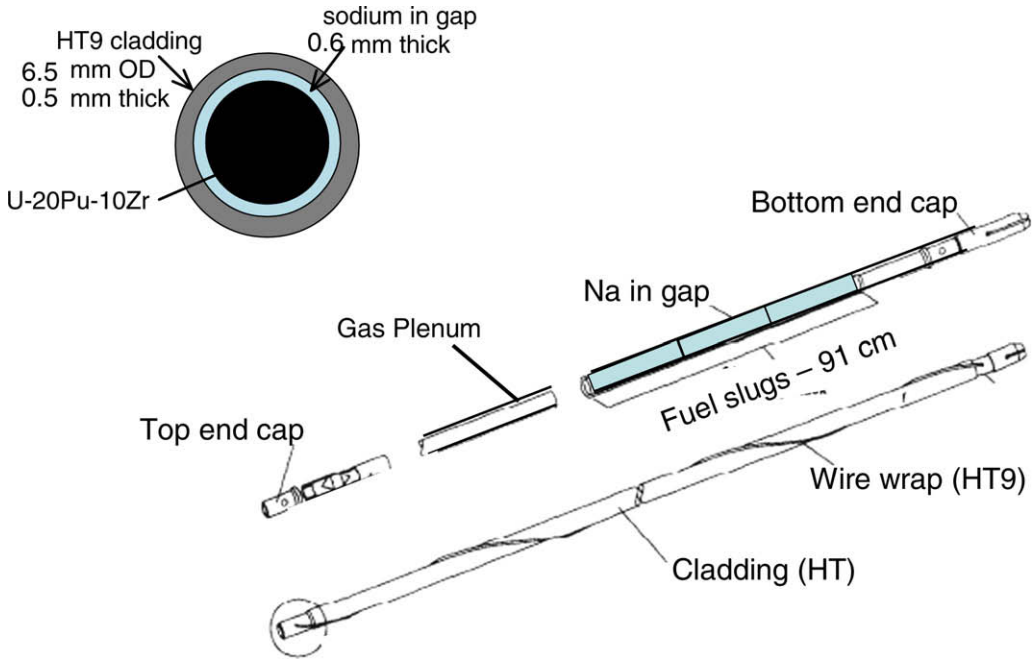

Fig. 21. Sodium fast reactor fuel pin.

8. Pyroprocessing

Instead of aqueous methods, metal fuel is reprocessed by non-aqueous, pyrometallurgical techniques (pyroprocessing) [23]. The motivations are the same as for aqueous reprocessing, namely separation of plutonium and the minor actinides from the other fuel components in order to prepare them for conversion to short-lived fission products. The efficiency of removing fission products from the recycle uranium is much lower than that from the aqueous process. The latter can be handled as if it were uranium from the ground, but the U product from pyroprocessing is sufficiently radioactive that it must be handled in a hot cell.

As Fig. 24 shows, the spent fuel from both LWRs and SFRs are treated by pyrometallurgical methods (electrorefining). The diagram represents an entire fuel cycle except for the enrichment in U-235 required for fuel fabricated for the LWR and the mining, milling and conversion of ore to U metal or oxide. The head-end step for LWR spent fuel is the same as in the UREX process, namely

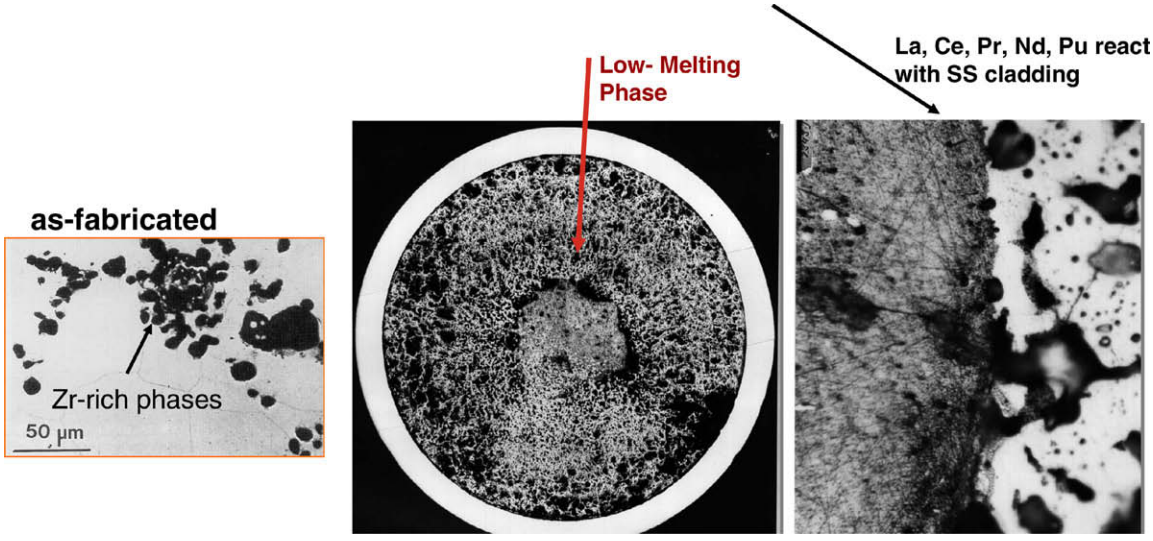

Fig. 22. Photomicrographs of SFR fuel before (left) and after irradiation (center and right).

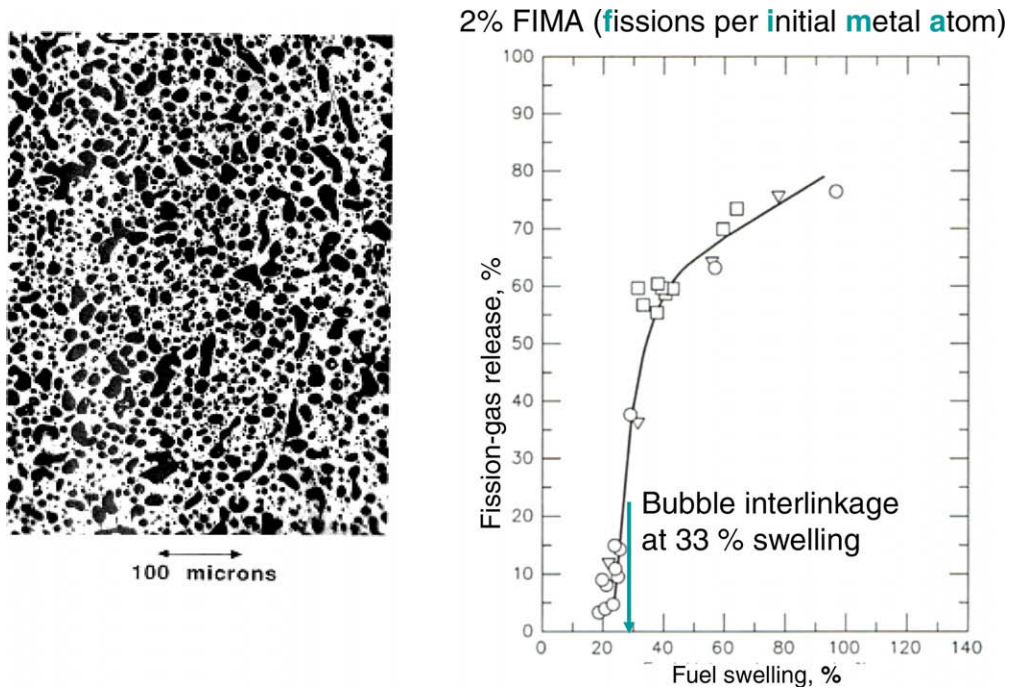

Fig. 23. SFR fuel irradiated to FIMA = 0.02.

a chop-leach operation that separates fuel from cladding[7] followed by conversion of the nitric acid leach solution containing all elements of the spent fuel to oxides. The oxide must be reduced to metal by reaction with lithium:

$$2Li + UO_2 \rightarrow 2Li_2O + U. \quad (21)$$

The contaminated U product is fed to an electrorefiner which separates uranium, plutonium plus minor actinides and all fission products from each other. The uranium product is recycled to a fuel element fabrication plant where fuel elements for the LWR(s) are made. The Pu + MA (TRU) product is fed to a second electrorefiner, which also receives as feed the chopped spent fuel slugs from the SFR. This unit separates out only the fission products; the heavy metals U and Pu and the minor actinides are recycled to the SFR to be burned. Plutonium and the minor actinides never leave the fuel cycle; uranium enters and electricity and fission products come out.

8.1. The electrorefiner

The electrorefiner, which is the heart of pyroprocessing, is shown in Fig. 25. This could also be called an *electrotransporter*, meaning that components are separated and moved to different locations. However, it is not electrolytic in the sense that an oxidized and reduced species are produced.

The system consists of an anode in the form of a basket into which are loaded the chopped fuel slugs from the SFR or the recovered metal from the LWR branch. The two cathodes are both at the

[7] If the fuel-cladding gap of LWR fuel were LM-bonded, the chop-leach step would be unnecessary. Since fuel and cladding never come in contact, the spent fuel should simply slip out of the cladding.

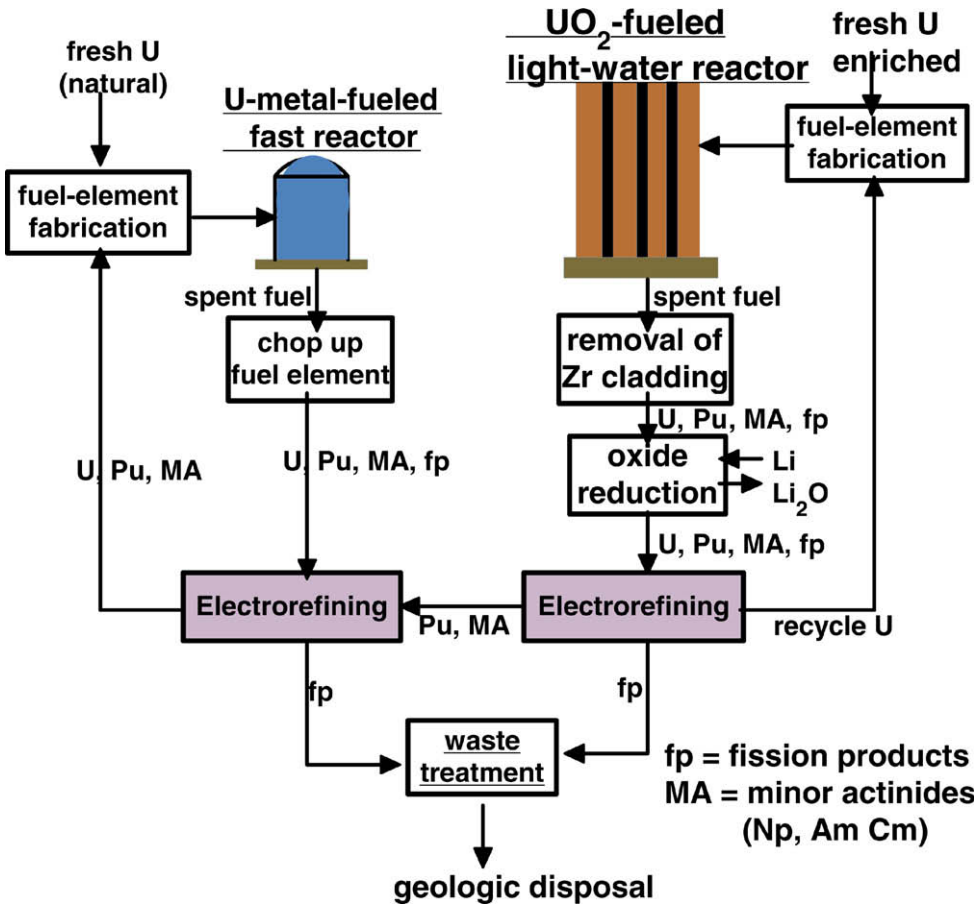

Fig. 24. Pyroprocessing of spent fuel from LWRs and SFRs.

same potential relative to the anode. The first one is stainless steel and the second one is a pool of liquid cadmium. Another pool of molten Cd occupies the bottom of the steel vessel which also contains the molten LiCl/KCl electrolyte. The eutectic temperature of LiCl and KCl is 350°, so the unit operates at ~500 °C.

The following separations are effected:

1. U^{3+} migrates to the first cathode where it is reduced to a very pure metal; none of the other components of the spent fuel codeposit.
2. Pu^{3+} and the minor actinide ions, are transported to the second cathode, where they are reduced to metals and dissolve in the Cd pool.
3. Alkali metals (Cs) and alkaline earths (Ba, Sr) and the rare-earths remain in the electrolyte.
4. The noble metals fall to the cadmium pool at the bottom of the vessel. The thermochemistry of the separation is analyzed below.

8.2. Electrode potential

For an adequate rate of electrotransport, the 'transportable' metal ion mole fraction in the electrolyte must ~0.02 [23]. All transportable ions from dissolution of the anode (see Fig. 25) are trivalent. The standard free energies of formation of the transportable ions at 500 °C range from −55 kcal/mole for UCl_3 to −62 kcal/mole for $PuCl_3$. The minor actinides fall between these values. Taking U as the major component, the anode reaction is:

$$U \rightarrow U^{3+} + 3e.$$

For which the standard electrode potential is obtained from:

$$\Delta G_f^o = -3\Im\varepsilon^o$$

where $\Im$ is Faraday's constant. With $\Delta G_f^o = -55$ kcal/mole, this formula yields $\varepsilon^o = 0.80$ V. The applied voltage is equal to the Nernst potential:

$$\varepsilon = \varepsilon^o - \frac{RT}{3\Im}\ln a_{U^{3+}}$$

neglecting nonideality, $a_{U^{3+}} \cong x_{U^{3+}} = 0.02$, so at $T = 773$ K, $\varepsilon = 1.0$ V. This is the voltage applied between the anode and the cathodes.

8.3. Why Pu does not deposit on the first cathode

The standard free energy of formation for $Pu \rightarrow Pu^{3+} + 3e$ is −62 kcal/mole, so the standard free energy for the reaction:

$$U^{3+} + Pu = U + Pu^{3+}$$

is $\Delta G^o = -7$ kcal/mole. The law of mass-action for this reaction is:

$$\frac{a_U^{cath} a_{Pu^{3+}}^{salt}}{a_{Pu}^{cath} a_{U^{3+}}^{salt}} = \exp\left(-\frac{-7000}{1.986 \times 773}\right) = 92.$$

For the U–20Pu–10Zr fuel:

$$a_{Pu^{3+}}^{salt} \approx 0.2 a_{U^{3+}}^{salt} \qquad a_U^{cath} \approx 1.$$

These activities yield an activity of plutonium metal in the uranium deposit of $a_{Pu}^{cath} = 0.002$ – thus explaining the high uranium purity on the first cathode.

8.4. How is Pu collected at the liquid Cd cathode?

The Nernst equation for the electrode reaction $Pu^{3+} + 3e = Pu(Cd)$ is:

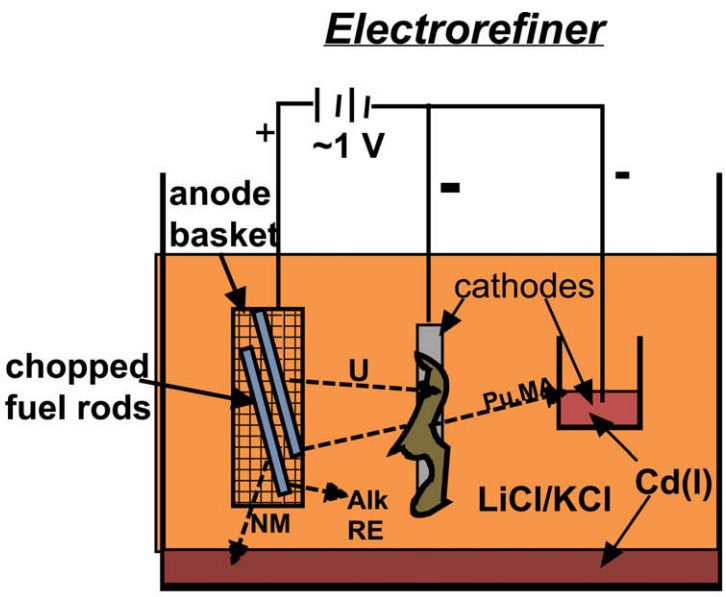

Stable (in salt phase)	Electro-transportable	Unstable (in Cd pool)
Cs, Ba, Sr	U, Pu, MA, RE	Mo, Pd, Rh, Ru

Fig. 25. Electrorefiner.

$$\varepsilon = \varepsilon^o - \frac{RT}{3\Im} \ln\left(\frac{a_{Pu^{3+}}}{a_{Pu}^{Cd}}\right)$$

where a_{Pu}^{Cd} is the activity of plutonium in liquid cadmium. For the same anode–cathode voltage ($\varepsilon = 1$ V) and the standard electrode potential for the Pu/Pu^{3+} couple ($\varepsilon^o = 0.9$ V) the above equation yields:

$$a_{Pu^{3+}}^{salt}/a_{Pu}^{Cd} = 0.13$$

Pu and Cd form the strongly bound intermetallic compound $PuCd_6$, which reduces the activity of Pu in the cadmium (but not its concentration) to 4×10^{-6}. Therefore the activity of Pu^{3+} in the salt is $0.13 \times 4 \times 10^{-6} = 5 \times 10^{-7}$. Neglecting nonideality, this is the mole fraction of Pu^{3+} in the salt adjacent to the second cathode, i.e., essentially zero. Thus the driving force for Pu^{3+} to be transported to the second cathode is its maximum value. When Pu^{3+} arrives at the second cathode, it is converted to the intermetallic compound and held in the liquid cadmium.

8.5. Why does not uranium collect in the second cathode?

Because it does not form an intermetallic compound as does plutonium.

9. Summary

The conventional fuel element for LWRs – UO_2 fuel, Zircaloy cladding, He bond – has been in continuous use for 50 years. Recently, economics-driven extension of fuel burnup has resulted in stresses on both the cladding and the fuel. Specific concerns are:

- strain from fission-product-driven swelling fuel,
- internal pressurization by fission gas released from fuel,
- internal stress-corrosion cracking by fission-product iodine,
- vibration-driven fretting degradation by grid spacers,
- external corrosion by coolant water,
- embrittlement by corrosion-product hydrogen.

Although the probability of cladding failure from these causes during the lifetime of a fuel element is low ($\sim 10^{-5}$), the consequences are not ($\sim$\$1 M/day if shutdown of the reactor is required and replacement power must be purchased). Nonetheless utilities and vendors resist even modest changes in fuel, such as a liquid–metal bond to replace helium in the fuel-cladding gap or replacing UO_2 or MOX fuel with a U–Zr hydride.

The next generation nuclear plant (Gen IV) likely to be the very-high-temperature reactor (VHTR). This reactor is fueled by tiny fuel particles (TRISO) embedded in graphite and cooled by helium. This reactor concept promises to deliver outlet coolant at temperatures approaching 1000 °C, which would make thermochemical hydrogen production or electrolysis of water economical. The UREX-1a reprocessing suite is needed to fulfill the requirements of nonproliferation and to avoid approaching limiting temperatures and site-boundary dose rates in the high-level waste repository. This collection of four distinct solvent extraction steps contained in UREX-1a, however, is far from being demonstrated.

Another candidate for the next generation nuclear plant is the sodium-cooled fast reactor (SFR). This reactor is intended to operate in coordination with one or more LWRs in a fuel cycle that accepts only fresh uranium and delivers only fission products and heat (electricity). The minor actinides and plutonium are recycled in the SFR until they are completely converted to fission products. The separation

process, called pyroprocessing, is based on an ingenious device called an electrorefiner, which is capable of recovering, albeit not at very high separation factors, all of the constituents of spent fuel, whether from the SFR, the LWR, or other reactors.

References

[1] G. Oudinet et al., J. Nucl. Mater. 375 (2008) 86.
[2] H. Kleykamp, J. Nucl. Mater. 324 (2004) 198.
[3] J. Turnbull, A Review of MOX Fuel and its Use in LWRs, OECD Halden Reactor Project, HWR-435, 1995.
[4] D. Olander et al., Nucl. Eng. Des., submitted for publication.
[5] M.T. Simnad, Nucl. Eng. Des. 64 (1981) 403.
[6] E. Greenspan et al., Nucl. Eng. Des., submitted for publication.
[7] D. Wongsawaeng, D. Olander, Nucl. Technol. 159 (2007) 279.
[8] A. Lillie et al., Zirconium Hydride Fuel Element Performance Characteristics, Atomics International/USAEC Rept. AI-AEC-13084, 1973.
[9] T. Besmann, T. Lindemer, J. Nucl. Mater. 130 (1985) 473.
[10] T. Besmann, T. Lindemer, J. Nucl. Mater. 137 (1986) 292.
[11] C. Guéneau et al., J. Nucl. Mater., these Proceedings.
[12] D. Petti et al., Modular Pebble-bed Reactor Project – Annual Report, Idaho National Laboratory, 2002.
[13] H. Kleykamp, J. Nucl. Mater. 206 (1993) 82.
[14] T.B. Lindemer, Thermochemical Analysis of Gas-cooled Reactor Fuels Containing Am and Pu Oxides, ORNL/TM-2002/133, Sect. 7.5, 2002.
[15] W. Thompson et al., Int. J. Mater. Res. 98 (2007) 10.
[16] A. Roine, Outokumpu HSC Chemistry for Windows, Chemical Reaction and Equilibium Software with Extensive Thermochemical Database, User's Guide Version 3.0, Outokumpu Research, Oy, Pori, Finland, 1997.
[17] D. Olander, Fundamental Aspects of Nuclear Reactor Fuel Elements, National Technical Information Service, 1976, (pp. 181–183, 156–157).
[18] T. Arai, J. Nucl. Sci. Technol. 17 (1980) 106.
[19] P.E. Potter, J. Nucl. Mater. 42 (1972) 1.
[20] K. Naito et al., J. Radioanal. Nucl. Chem. Art. 143 (1990) 221.
[21] F. Homan et al., Nucl. Technol. 35 (1977) 428.
[22] R. Wigeland et al., Nucl. Technol. 154 (2006) 95.
[23] J. Battles et al., Pyrometallurgical processes for recovery of actinide elements, in: International Symposium on Actinides: Processing and Materials, San Francisco, CA, 1994.